Finanziato dall'Unione europea NextGenerationEU | Ministero dell'Università e della Ricerca | Italiadomani PIANO NAZIONALE DI RIPRESA E RESILIENZA

multi-Risk sciEnce for resilienT commUnities undeR a changiNgclimate

Codice progetto MUR: **PE00000005** – C93C22005160002

Deliverable title: Development of surface water models and groundwater models to generate deterministic/probabilistic scenarios based on climatic projections and seasonal meteorological predictions

Deliverable ID: 1.3.3

Due date: 1.06.2024

Submission date: : 1.06.2024

AUTHORS

Jost von Hardenberg, Alberto Viglione, and Stefania Tamea (POLITO); Stefania Da Pelo, Giulio Vignoli, Antonio Coppola (UNICA) Matteo Camporese, Pietro Teatini (UNIPD); Luigi Piemontese (UNIFI), Maria Cristina Rulli (POLIMI), Giacomo Bertoldi (Eurac Research), Simone Gabellani, Roberto Rudari (Cima Foundation

1. Technical references

Project Acronym	RETURN
Project Title	multi-Risk sciEnce for resilienT commUnities undeR a changiNg climate
Project Coordinator	Domenico Calcaterra UNIVERSITA DEGLI STUDI DI NAPOLI FEDERICO II domcalca@unina.it
Project Duration	December 2022 – November 2025 (36 months)

Deliverable No.	DV1.3.3
Dissemination level*	
Work Package	WP3 - Drought risk under environmental and climatic changes
Task	T3.2 - Drought hazard modelling
Lead beneficiary	Cima Foundation)
Contributing beneficiary/ies	UNIPD, POLITO, UNIFI, EURAC, CIMA, POLIMI.

* PU = Public

PP = Restricted to other programme participants (including the Commission Services)

RE = Restricted to a group specified by the consortium (including the Commission Services)

CO = Confidential, only for members of the consortium (including the Commission Services)

Document history

Version	Date	Lead contributor	Description
0.1	24.05.2024	Pietro Teatini (UNIPD)	First draft
0.2	27.05.2025	Jost von Hardenberg (POLITO	Critical review and proofreading
0.3	30.05.2024	Roberto Rudari (CIMA)	Edits for approval
1.0	31.05.2024	Francesco Ballio (POLIMI)	Final version

2. ABSTRACT

This report summarizes the contributions to the Deliverable DV 1.3.3, focused on the development of surface water models and groundwater models to generate deterministic/probabilistic scenarios based on climatic projections and seasonal meteorological predictions.
This deliverable focuses on the development, calibration, and validation of models that will be used in DV 1.3.4 for seasonal forecasts and/or climate scenarios.
Format: Methodological report and algorithms (month 18).

The contributions cover various aspects of water resource management and hydrogeological research:
A3.3.1 addresses coastal aquifer salinization, emphasizing the complex environmental factors contributing to saline intrusion and proposing a methodological approach for understanding recharge sources, flow pathways, and salinization processes. It presents a case study in the Flumendosa plain in southeast Sardinia, including geological surveys, hydrogeological modeling, and preliminary results indicating the impacts of withdrawals and climate change on saline intrusion.
A3.3.2 examines the impact of irrigation practices on water balance and groundwater recharge in Veneto, in response to the European Water Framework Directive's requirements to reduce agricultural water use. Using the CATHY model, which integrates surface and subsurface hydrology, the study simulates overland and subsurface flow and solute transport. This research aims to understand the qualitative and quantitative effects on groundwater, which is crucial for drinking water supply and irrigation in the region.
A3.3.3 describes the use of the SWAT+ model to simulate drought conditions in the Arno Basin, considering current and future climate change scenarios. The focus is on agricultural variables related to drought and includes methods for model setup and next steps for simulation.
A3.3.4 analyzes spring discharge data and meteorological parameters to develop a model predicting spring discharge for different precipitation scenarios. The analysis involves evaluating the relationship between various meteorological indexes and spring flow rates, aiming to create a multi-parametric model for estimation.
A3.3.5 develops agro-hydrological models to quantify agricultural drought hazards in Italy. This work distinguishes between different types of drought and centers on agricultural drought, which affects crop yields. The objective is to create a detailed model of crop-specific water demands and deficits across Italy, enhancing spatial and temporal resolution and crop identification accuracy.
A3.3.6 uses 2D and 3D hydrodynamic models to understand the small-scale onshore effects of climate change that we can only predict on a much larger scale (compared to what is necessary to analyze these coastal structures).
A3.3.7-A3.3.8-A3.3.9 investigates secondary soil salinization in coastal areas due to irrigation with saline groundwater. Activity A3.3.7 focuses on the morphological and physical-chemical characterization of soil profiles to assess salinization processes. Activity A3.3.8 involves hydraulic characterization of these soils to further evaluate salinization impacts. Activity A3.3.9 uses a 1D agro-hydrological model to simulate water and salt distribution in the soil under varying climatic scenarios, considering the progressive salinization of groundwater from marine intrusion. These simulations provide critical data on water and salt dynamics and percolation flows towards the aquifer.
A3.3.10 introduces a set of tools used to summarize the main properties of extreme droughts, with the goal of subdividing the events in groups characterized by similar properties. The proposed procedure allows for a drought classification that can be used for better understanding the mechanisms beyond these events.
A3.3.11 focuses on model-based drought monitoring in hydrology to assess and predict drought conditions. The approach involves three key steps: first, hydrological modeling is used to spatially map relevant hydrological state variables. Second, the correlation of hydro- and meteorological variables with historical drought observations helps to identify patterns and correlations. Finally, the developed drought hazard modeling framework is applied to future scenarios to improve drought prediction and management.
A3.3.12 discusses the coupling of seasonal forecast data with machine learning techniques for reservoir operation and management in regions facing water scarcity. It outlines the development of a Decision Support System (DSS) using a NARX model trained on Sicilian reservoir data, aiming to predict reservoir volumes up to six months ahead to support water resource management decisions.

3. Table of contents

1. Technical references 2
Document history 3
2. ABSTRACT 4
3. Table of contents 5
List of Tables 6
List of Figures 6
4. Groundwater models 9
4.1 Hydrogeological modelling of coastal catchments and saltwater intrusion in Sardinia. 9
4.1.1 Introduction 9
4.1.2 Study area 9
4.1.3 Methodological approach 10
4.1.4 Preliminary results 11
4.1.5 Conclusions 13
4.2 Development of integrated models of the Venetian high plain aquifers to map current recharge fluxes 16
4.2.1 Introduction 16
4.2.2 Study area, input data and model calibration 16
4.2.3 Irrigation ad recharge simulations 17
4.3 18
4.3.1 Morphological and physico-chemical characterization of selected soil profiles 19
4.3.2 Hydraulic characterization of selected soil profiles 21
4.3.3 Physically-based dynamic simulations with a 1D agro-hydrological model 22
5. Surface water models 25
5.1 Hydrological models for the quantification of hydrological drought hazards at seasonal and climatological scale in the Po watershed and Arno watershed 25
5.1.1 Context 25
5.1.2 The Continuum model 25
5.1.3 Model setup and calibration 25
5.1.4 Results 26
5.2 River low-flow and intermittency modelling and spring modelling in North-Western Italy 28
5.3 Development of agro-hydrological models for the quantification of agricultural drought hazards. 29
.5,3.1 Introduction 29
5.3.2 Model development 30
5.4 Modelling the hydrodynamic of the shallow regions under water scarcity conditions: during drought periods shallow regions are deeply affected by seasonal conditions 31
5.4.1 Introduction 31
5.4.2 Materials and methods 32
5.4.3 A potential case of use to start testing: Stagnone di Marsala (Sicily) 34

5.5 Quantifying the drought hazards via multivariate statistics, and analysis of specific drought events. 35
5.5.1 Introduction 35
5.5.2 Materials 35
5.5.3 Methodology 35
5.5.4 Results 36
5.6 Development and integration trough machine learning of model ensembles informed by HR remote sensing products for understanding drought formation process (snow drought versus increased evaporative demand) in Alpine regions (i.e. Adige catchment). 38
5.6.1 Overview 38
5.6.2 Phase 1: Modeling for Spatial Mapping of Relevant Variables in the Adige Catchment 38
5.7 Coupling of seasonal forecast data and machine learning techniques for reservoir operation and management in a context of water scarcity in Sicily/Southern Italy. 40
5.7.1 Introduction 40
5.7.2 Methods 40
5.7.3 Study Area and Datasets 41
5.7.4 Preliminary Results 41
5. Conclusions 44
6. References 45

List of Tables

Table 1. Grouping of soil profiles for each map unit 20
Table 2. The table reports the travel time (in years) required for the 25, 50, 75 and 100% of the specific input mass (M0=0.01 g/cm2) to reach the GW, for the profiles where the depth to GW is lower than 10 m. 22

List of Figures

Figure 1: Geological map of the Muravera plain. www.SardegnaGeoportale.it 10
Figure 2 Main workflow within the framework of the Return project 11
Figure 1. Piezometric change between August 2020 and January 2021 (a) conductivity depth profile deep wells (b) salt edge extension (c) 12
Figure 4. Recharge variation simulated with the SWB from 2000 to 2100 13
Figure 5. Salt wedge variation perpendicular to the coast (section NW-SE in Figure 3b) 14
Figure 6. Comparison of salt wedge variation perpendicular to the coast with and without withdrawals 15
Figure 7: Veneto Region and study area position 16

Figure 8 scatter plot of observed vs simulation hydraulic head (left) for the uncalibrated model, and (right) for the calibrated model 17

Figure 9a) Mean spatial recharge [l/s ha] simulated over the irrigation season 2018/05/31 - 2018/08/31 and b) difference between the mean spatial recharge of the current irrigation scenario (flood and sprinkler) and the future scenario (sprinkler only). 18

Figure 10. Study area (in green) and the investigated soil profiles 19

Figure 11. Distribution of prevailing soils in the study area (modified by AGRIS et al., 2014). 20

Figure 12. Sand, silt, and clay content of the surface horizon produced by ordinary Kriging 21

Figure 13. Whole set of cumulative breakthough curves at 1 m depth simulated by FLOWS for all the soil profiles investigated. The thick red curve represents the average curve 24

Figure 14: Overview of the study area: maps with (a) elevation, (b) climate, (c) land cover types, and (d) location of the model domain, modelled river network (dark blue line), and study sub-catchments outlets (grey dots, with black edge if used in model calibration 27

Figure 15: Streamflow (Q) model performances for the model calibrated during average climatic conditions: KGE values on monthly Q during wet years (a), moderate droughts (b), and the severe drought (c) for each study sub-catchment, and their distributions as boxplots (d) grouped by calibration (full colours) and evaluation (light colours) sub-catchments 27

Figure 16: Summary of model performances for the model calibrated during a drought: KGE values on monthly Q over moderate droughts (a) and the severe drought (b) for each study sub-catchment, their distributions as boxplots (c) grouped by calibration (full colours) and evaluation (light colours) sub-catchments, maps of r and nRMSE on monthly ET standardized anomalies over moderate droughts (d and g) and the severe drought (e and h), and errors distributions as boxplots per each land cover types (f and i). Water bodies and urban areas were excluded from the comparison. Model outputs were rescaled by bilinear interpolation to the resolution of the LSASAF product for comparison 28

Figure 17: Left: Determination coefficient between SRI and other indexes for different seasons (Fuse case). Right: Correlation matrix between spring monthly discharge and cumulative precipitations for different period (1-6 months, Fuse case 29

Figure 18: Blue water consumption for Italy assessed with the agro-hydrological model WATNEEDS 31\

Figure 19: Example of the procedure adopted to summarize the main directions ofevolution of an event. The two maps show the area interested by the drought in twosuccessive time steps (namely 1 and 2), whereas the centroid at step 1 is reported over the area in step 2 to identify the expansion in each of the 8 main directions 36

Figure 20: Normalized Area - Time Accumulation (NATA) curves for all the events, and separating between events during the cold, warm and mixed period. Grey lines represent the NATA curves for the individual events, the bold lines depict the mean behaviors, whereas the dashed lines mark +/- one standard deviation 36

Figure 21: Characteristics of the two clusters of drought events identified using the PAM method 37

Figure 22: Starting location of drought events: a) all events, b) events of group 1, c)events of group 2 38

Figure 23 – Control panel of the tool developed for the AdB 42

Figure 24 – NARX models results for the SF release of September 2023 43

Figure 25 – NARX models results for the SF release of December 2023 43

.

4. Groundwater models

4.1 Hydrogeological modelling of coastal catchments and saltwater intrusion in Sardinia.

This activity summarizes four contributions, previously indicated as

- A 3.3.1a Collection of large-coverage and dense geophysical measurements over a Sardinian coastal catchment affected by saltwater intrusion and groundwater overexploitation.
- A 3.3.1b Development of a geological model of the Sardinian coastal catchment. The geomodel relies on the geophysical model (cf. A 3.3.1a) and incorporates all the available, different pieces of information.
- A 3.3.1c Development of the hydrogeological model based on the geological and geophysical models available for the coastal catchment (cf. A 3.3.1a and A 3.3.1b). Implementation of the associated scenario analysis under climate and societal changes.
- A 3.3.1d Development of monitoring and early warning systems aiming at redirecting the usages of surface and groundwater resources to reduce exacerbation of saltwater intrusion.

4.1.1 Introduction

Coastal aquifer salinization is a critical environmental concern stemming from various factors, posing substantial threats to water resources and ecosystems. In this project, we plan to experiment with a methodological approach to enhance knowledge on recharge sources, flow pathways, surface- and groundwater interaction, and residence times in coastal aquifers affected by saltwater intrusion to develop targeted management strategies. In-depth geological and hydrogeological surveys, complemented by a geochemical and isotopic approach, offer insights into aquifer physical properties, recharge areas, and salinization processes. Nevertheless, stratigraphic information in depth is often site-specific and requires interpretation for upscaling. Reconstructing geological settings in three dimensions in coastal alluvial environments is complex due to non-linear transgressive and regressive depositional dynamics. Extensive and dense geophysical measurements in coastal catchments impacted by saltwater intrusion and groundwater can enhance hydrogeological models for improved resource management under anthropogenic and climate stresses.

4.1.2 Study area

The coastal area of the Flumendosa plain in southeast Sardinia (Italy) has been selected as a pilot site. Saltwater intrusion (due to anthropic activities altering the natural hydrodynamic equilibrium between groundwater, surface water, and seawater) has affected it since the 1950s. In this coastal plain, water supply for the socio-economic development of local communities has always relied on groundwater abstraction. During summertime, when water demand rises due to irrigation and tourism, uncontrolled groundwater exploitation occurs. Moreover, the reduction of runoff water due to the occurrence of several dams along the watershed, are leading to a further extension of the saltwater intrusion. Salinization of surface- and groundwater and land traditionally used for agriculture has resulted in several environmental, economic, and social issues. The Flumendosa is the second longest river in Sardinia (122 km) and flows across the plain area for its last ten kilometers before reaching the Tyrrhenian Sea. 22The plain mostly consists of ancient to actual quaternary alluvial and continental deposits hosting a complex hydrogeological system. It is characterized by the presence of a 50-meter-thickness alluvial phreatic aquifer, locally confined by silty clay lenses with variable extension and thickness (Arras et al., 2019). Low-productive aquifers hosted in the Upper Pleistocene conoids and the Paleozoic metamorphic basement (Figure 3) can contribute laterally to recharge the alluvial aquifer.

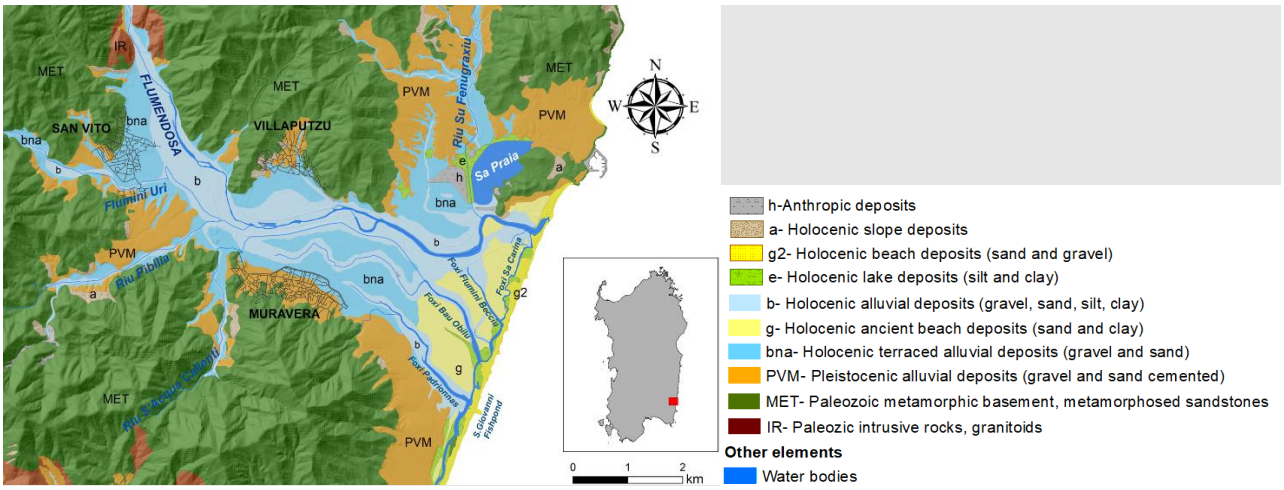

Figure 3. Geological map of the Muravera plain. www.SardegnaGeoportale.it.

4.1.3 Methodological approach

All data from previous fundamental studies were collected, organized, and systematized to optimize a robust geological and hydrogeological conceptual model (DSCG-STGRI, 2018), focusing on missing knowledge elements to support the subsequent development of an underground water resource management system. As outlined in Figure 4, the work focused on three specific objectives: i) describing the groundwater flow field and the main geochemical processes determining its qualitative characteristics, defining the extent of the salinized aquifer portion, and identifying the main contributions to the alluvial aquifer recharge; ii) quantifying natural recharge and aquifer response times; iii) identifying the dynamics and evolution of salinization. To this end, an innovative multidisciplinary methodological approach was applied, combining traditional hydrogeological and modeling techniques with geochemical and isotopic techniques.

To achieve the first objective, hydrogeological, geochemical, and multi-isotope characterization of the plain was carried out through monitoring, sampling, and water dating (Porru et al., 2024). Estimation of natural recharge was performed using two methodologies: the application of the Soil Water Balance code (SWB) and the Water Table Fluctuation (WTF) method (Porru, 2023; Porru et al., 2021). Finally, to describe saline intrusion and simulate its evolution over time, the collected data were inserted into a numerical hydrogeological model implemented using the innovative IMOD-python code, which respected all geological characteristics of the site (Porru, 2023). To implement the model, electrical conductivity depth profiles were obtained from several wells and piezometers to reconstruct surfaces delineating the interface between freshwater (EC < 2 mS/cm) and brackish water (2 mS/cm < EC < 30 mS/cm), and that between brackish water and saline water (Da Pelo et al., 2022). These surfaces were generated by interpolating measured data from actual monitoring points and fictitious data inserted at scattered points in the remaining part of the domain to spatially distribute freshwater inland. Simulation of scenarios has been applied taking into account the variation of recharge over time using the methods described in (Da Pelo et al., 2021; Porru et al., 2021).

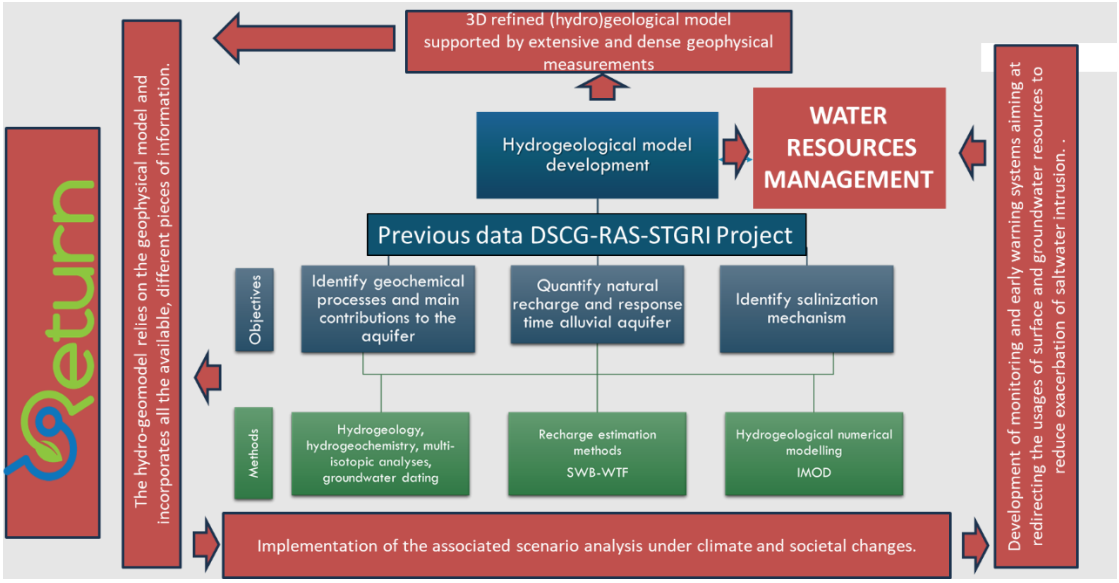

Figure 4. Main workflow within the framework of the Return project

On top of that, the collection of airborne electromagnetic data[5] aims to optimize and reconstruct the complex hydrogeology of the coastal aquifers, filling the knowledge gaps necessary to design early-warning systems and to guide salinization mitigation strategies. The geophysical data will allow, for example, the reconstruction of subsurface electrical resistivity up to approximately 100 meters deep, with a resolution that can be a few tens of meters in shallow portions. The geophysical model can serve as a reliable foundation for the (hydro)geological model used for scenario analysis.

[5]4.1.4 Preliminary results

In the alluvial aquifer, piezometric heads gently decrease from approximately 8 meters above sea level (asl) in the north-western part of the plain towards the sea with a medium gradient of 1‰. In the conoidal aquifer, the hydraulic gradient is much steeper (13‰) and reaches values of 18 meters asl. Interactions between the Flumendosa River and groundwater vary along the plain. Figure 6a shows that in the north-western part, the Flumendosa River drains the aquifer, while in the central part of the plain, downstream of Villaputzu village, the trend is reversed, and the aquifer discharge into the Flumendosa River. Recharge from the Flumini Uri River to the aquifer is also observed. The water table's zero level is approximately 2 kilometers from the inland shoreline during the winter. In the summer, the piezometric head decreases by about 1.5 meters across the entire plain, and the zero level moves inland by about 1 kilometer.

The monitoring of electrical conductivity at approximately 30 meters deep boreholes shows that the depth of the salt wedge varies between -15 masl and -35 masl. In the north area of the Muravera Plain, the position of the interface doesn't change significantly. In the central sector of the plain, under unconfined conditions, the deepening of the interface occurs as the piezometric head increases. The depth of the saline wedge appears to be shallower near the abandoned branches of the river currently totally salinized (Figure 6b, c).

[7]The preliminary processing and interpretation of airborne magnetic measurements together with the electromagnetic data are still ongoing. However, a general good matching of the salinized area delimited through field measurements with that highlighted with electromagnetic data can be already observed.

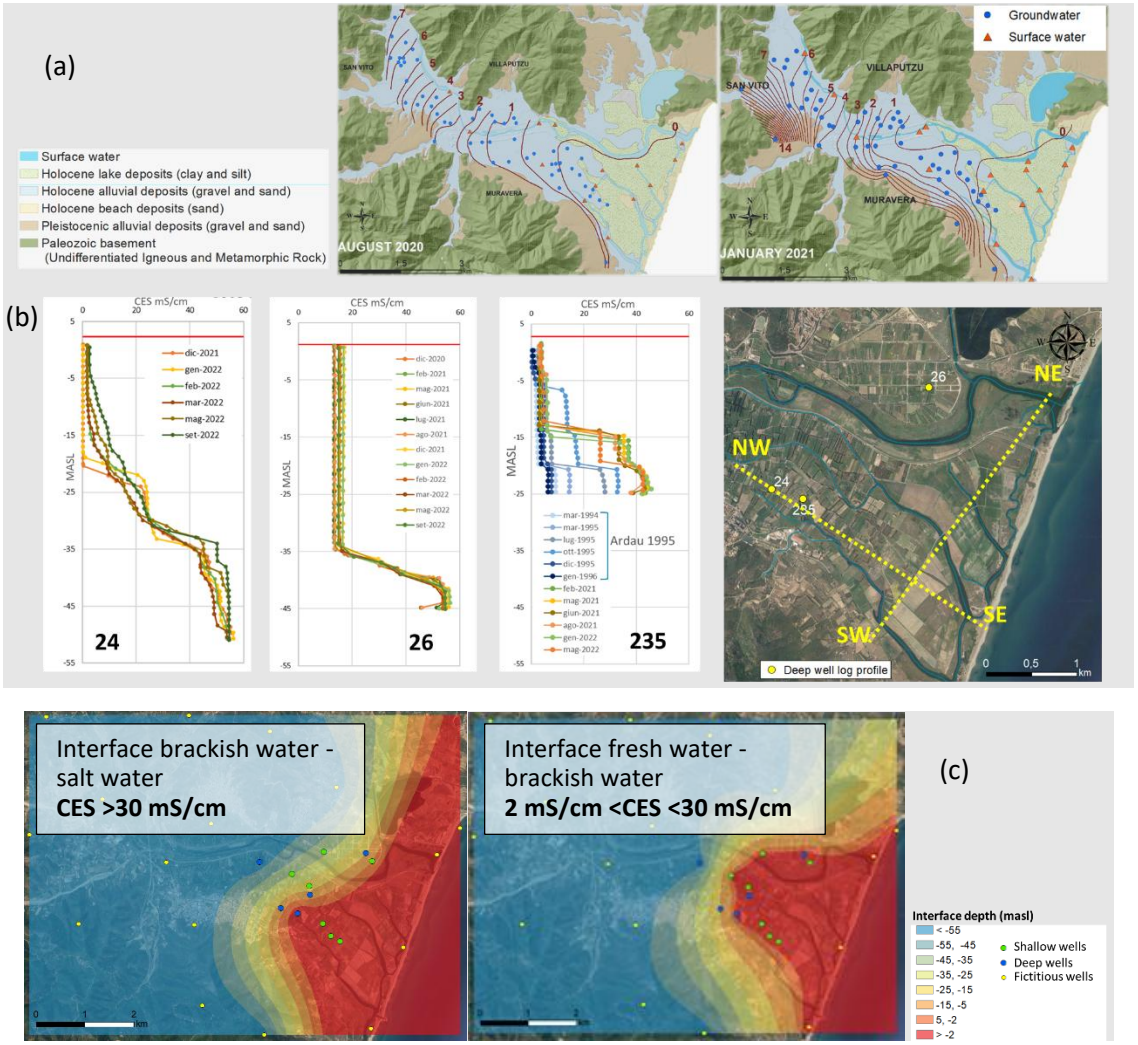

Figure 6. Piezometric change between August 2020 and January 2021 (a) conductivity depth profile deep wells (b) salt edge extension (c)

The simulation on recharge variation from 2000 to 2100 reveals that a progressive decrease in precipitation corresponds to a significant decrease in recharge as well. Recharge values decrease from exceeding 3 Mm^3 to less than 0.5 Mm^3 (Figure 8).

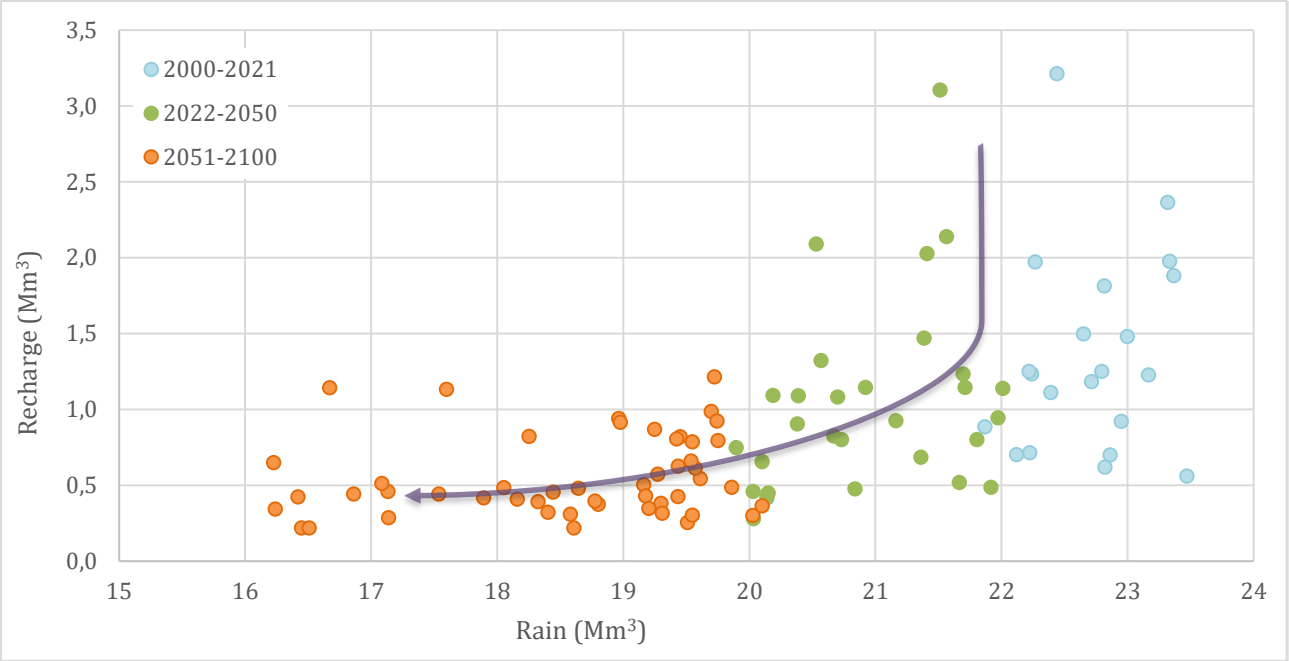

Figure 8. Recharge variation simulated with the SWB from 2000 to 2100

The simulation model of salt wedge variation over time in the Muravera plain is reported in Figure 9*10* and Figure 11. It is important to note that the results are preliminary, as they are derived from an uncalibrated model and represent a simulation using average values without considering seasonal variations and some relevant boundary conditions such as widespread irrigation wells. Nevertheless, initial analyses can be conducted on the trend of saline intrusion and the impacts of natural recharge variation and withdrawals on the freshwater-brackish water and brackish water-saline water interfaces.

Figure 9 *10*illustrates the variations of the salt wedge over time*5*. Generally, there is a progressive rise of the salt wedge over time, eventually reaching the level of the piezometric head.

To analyse the effect of withdrawals on the dynamics of the salt wedge, a simulation was conducted without including withdrawals in the model. As shown in Figure 11, reducing withdrawals would result in a decrease in the expansion of the saline intrusion towards the inland areas.

4.1.5 Conclusions

The collection and utilization of existing data in a double-density flow and transport numerical model offer a preliminary description of potential scenarios for 2050 and 2100. Geophysical electromagnetic and magnetic data will further optimize the geo-hydrogeological model, enhancing the reliability of the produced data.

Effective management and prevention of coastal aquifer salinization heavily depend on a thorough understanding of geological and hydrogeological dynamics. Integrating this knowledge into mitigation strategies ensures a more accurate and tailored approach to safeguarding water resources. Given ongoing anthropogenic stresses and climate change impacts on coastal aquifers, prioritizing geological and hydrogeological research is paramount for sustainable water management.

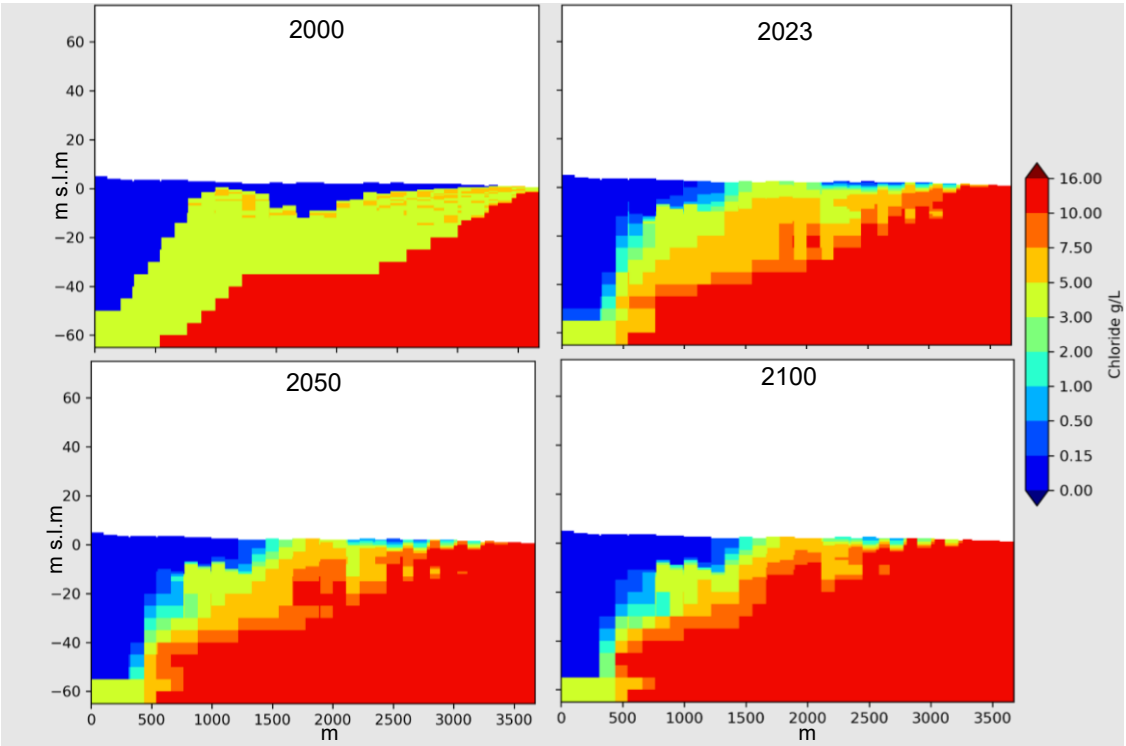

Figure 9. Salt wedge variation perpendicular to the coast (section NW-SE in Figure 6b)

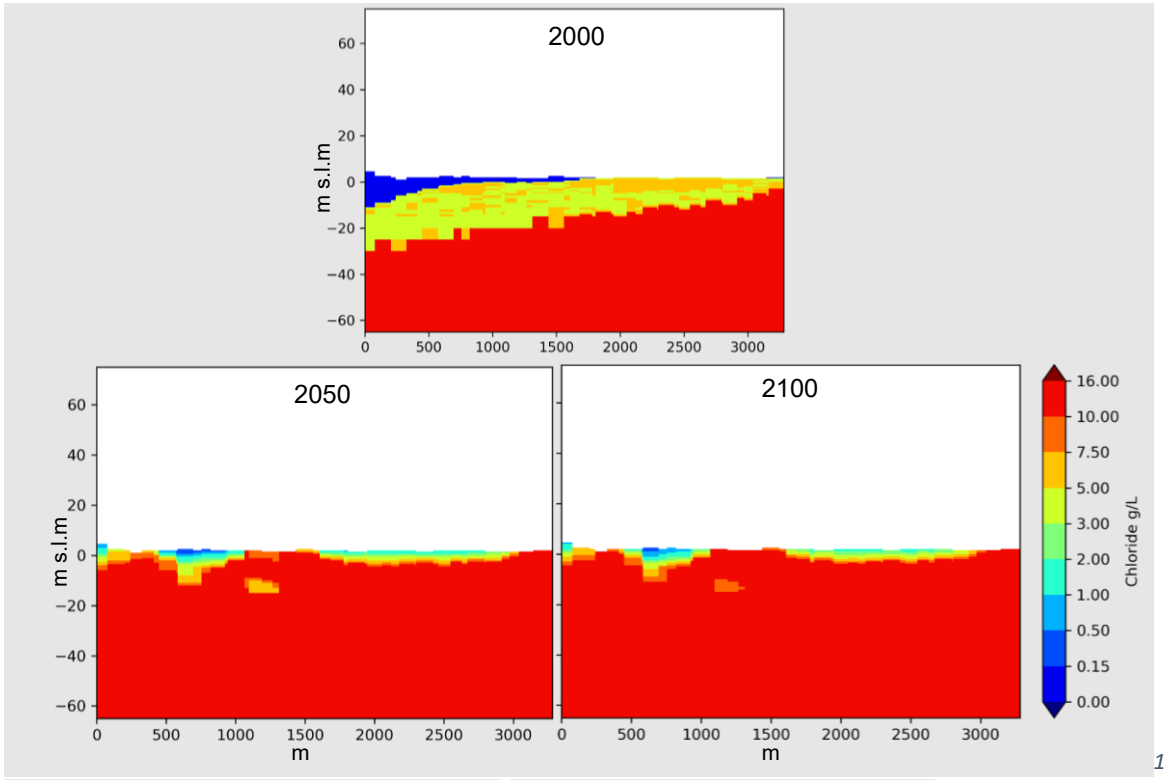

*10*Figure 6

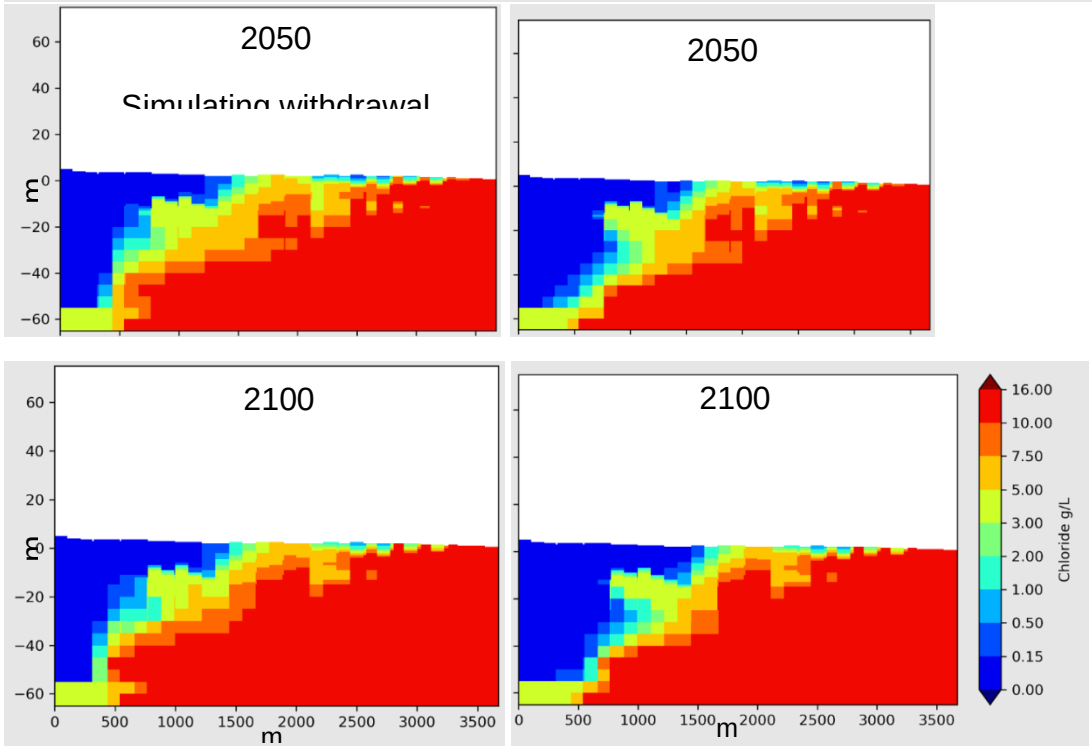

Figure 11. Comparison of salt wedge variation perpendicular to the coast with and without withdrawals.

4.2 Development of integrated models of the Venetian high plain aquifers to map current recharge fluxes

4.2.1 Introduction

The scientific question at the basis of this activity originates from the European Water Framework Directive, which, among other things, requires a reduction in the amount of water used in agriculture to guarantee the ecological flow of rivers. To meet these requirements, irrigation techniques must be reviewed in order to save water. It would be important to understand what the qualitative and quantitative impact on the water balance will be, in particular on the groundwater recharge, since groundwater in Veneto represents the main drinking water supply and irrigation represents an important fraction of the groundwater recharge.

To study these aspects, CATHY, an integrated surface-subsurface hydrological model, is being used. CATHY is a physically based model that simulates the overland and subsurface flow by coupling a finite element solver for the 3-D Richards equation for the variably saturated porous media with a finite difference solver for the 1-D zero-inertia approximation of the shallow water equations for surface flow. It also couples a 3D advection-dispersion equation with a 1D advection-diffusion equation for solute transport in the subsurface and surface, respectively.

4.2.2 Study area, input data and model calibration

The study area (Figure 7) is located in Veneto, a region in the northeast of Italy that is characterized by an important agricultural tradition. Its extension is about 900 km^2. It is delimited to the northeast by the Piave river, to the west by a flow line parallel to the Brenta river, to the south by the Risorgive area - a zone of groundwater resurgence - and to the north by the Montello and Asolo hills. In this activity, attention was focused on the shallow unconfined aquifer and 28 wells (ATS, ETRA, VERITAS, ARPAV and SAN BENEDETTO), for which water level time series are available, were used for calibration.

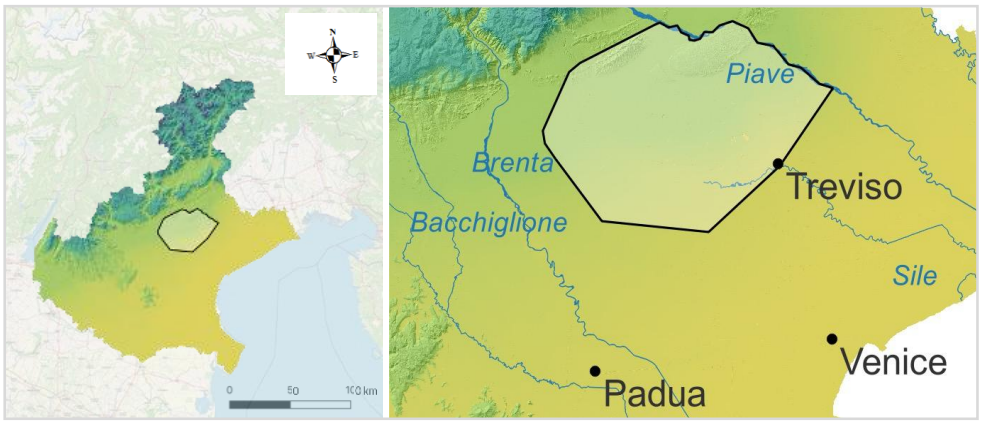

Figure 7: Veneto Region and study area position.

The rainfall data were downloaded from the ARPAV website. The evapotranspiration coefficients were evaluated using the Penman-Monteith equation, based on the soil use indicated by the 2012 Carta di copertura del suolo of the Veneto Region. The irrigation data were provided by the Consorzio di Bonifica Piave. The soil use distribution introduced was obtained from the shape file of the 2012 Carta di copertura del suolo of the Veneto Region. In the study area, the most prevalent land uses are arable land (42%) and urban centers (29%). These data align with the economic traditions of the Veneto region, which are heavily reliant on agriculture. However, they also reflect a concerning trend of reducing the area suitable for agriculture, with an increase in urban and industrial areas.

The model calibration was conducted by alternating the use of FeFlow and CATHY. The involvement of FeFlow was necessary because it has FePEST already implemented and allows for a straightforward utilization of the pilot points method, which in CATHY would have necessitated a significant amount of time to implement.

The initial FePEST calibration step was conducted in order to obtain a more realistic unconfined aquifer bottom, which had previously been assumed to be either parallel to the surface or flat. The calibration process incorporated data from the ISPRA (Italian National Research Institute) stratigraphical database, which indicates that the unconfined aquifer reaches a maximum depth of -40 m a.s.l. Next, the heterogeneous hydraulic conductivity field was obtained in two steps. Initially, a steady-state calibration was performed with FEFLOW. Subsequently, a refined transient state calibration was conducted with CATHY, coupled with the Shuffled Complex Evolution – University of Arizona algorithm.

Figure 8 presents a comparison between the uncalibrated and calibrated simulation results. Figure 8a depicts the scatterplot of the 28 wells obtained from the simulation data with uncalibrated hydraulic conductivity (K_s) and uncalibrated bottom. In this instance, approximately half of the wells' levels are overestimated in comparison to the observed data, with a total root mean square error (RMSE) of approximately 27 m. Figure 2b illustrates the scatterplot of the calibrated model. In this instance, the degree of head overestimation is reduced, and the RMSE is also diminished to one-third of its previous value. Following calibration, a validation step was also performed.

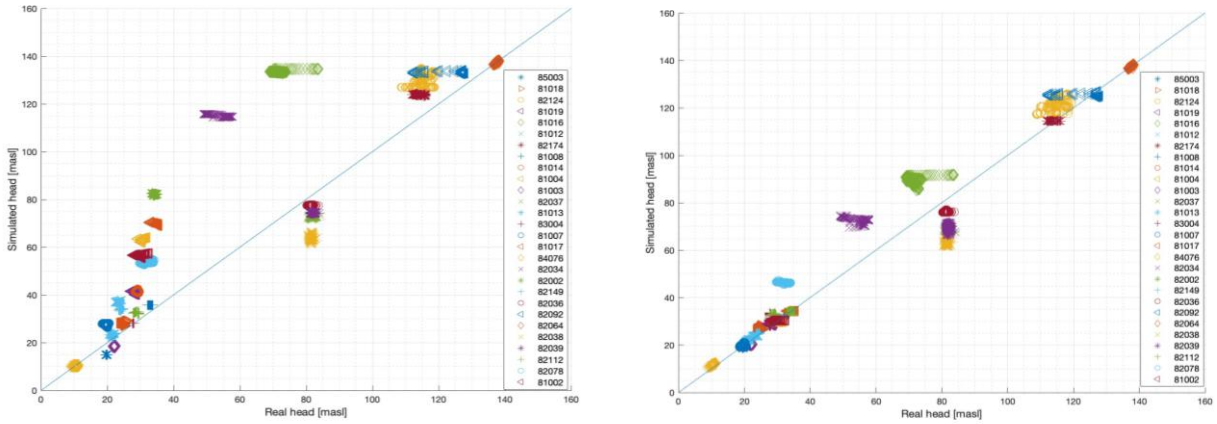

Figure 8 scatter plot of observed vs simulation hydraulic head (left) for the uncalibrated model, and (right) for the calibrated model.

4.2.3 Irrigation ad recharge simulations

Having calibrated and validated the model, it was possible to perform a simulation of the irrigation variation scenario. The flood irrigation method, which is prevalent in this region, necessitates the withdrawal of considerable quantities of water, particularly from the Piave river. However, the irrigation excess contributes to groundwater recharge. In accordance with the European Water Framework Directive, this type of irrigation is being converted to sprinkler irrigation, which in theory would reduce the waste of this precious resource.

To assess the quantitative impact that this planned irrigation method change will have on the groundwater recharge, we set up a simulation with reduced irrigation rates in the areas that will be affected by the irrigation method variation and corresponding increased water levels in the Piave River. The rating curve for the Piave river was constructed using data from ARPAV, while the irrigation data were obtained from the Consorzio di Bonifica Piave. In the case of flood irrigation, the discharge value is approximately 1.86 l s^{-1} ha^{-1}, while in the case of sprinkler irrigation, the discharge value is approximately 0.62 l s^{-1} ha^{-1}. The difference between the two discharges, multiplied by the area under flood irrigation, provides an estimate of the discharge that was assumed to be derived from Piave. This estimate can be used to calculate an approximate water head increase. This information was employed to modify the boundary conditions of the Piave river, in conjunction with the

atmospheric forcing during the irrigation period, which commenced on May 31st and concluded on August 31st, 2018.

The wells that exhibit discernible effects of the irrigation variation are those currently undergoing flood irrigation. The water head exhibited a slight decrease with respect to the sprinkler and flood irrigation case, with an average reduction of 0.5 m per well. The total cumulative recharge of the aquifer over the entire domain was directly computed by the CATHY model, resulting in a difference between the base case and the case of irrigation variation approximately -10%, corresponding to a 50% reduction in water withdrawals from the Piave River.

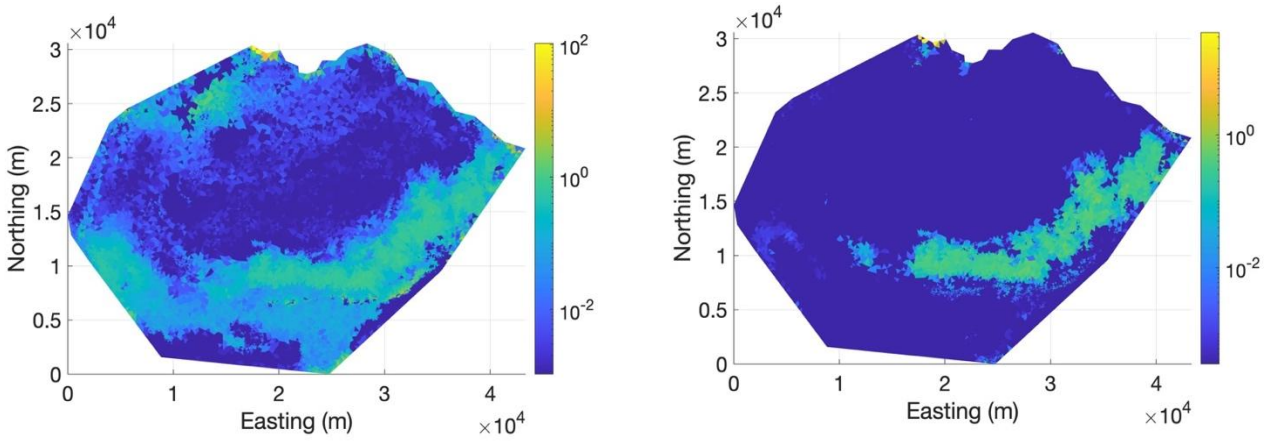

Figure 9a) Mean spatial recharge [l/s ha] simulated over the irrigation season 2018/05/31 - 2018/08/31 and b) difference between the mean spatial recharge of the current irrigation scenario (flood and sprinkler) and the future scenario (sprinkler only).

A final analysis was conducted to evaluate the time-averaged spatial distribution of recharge over the domain (Figure 9). This analysis revealed that the spatial contribution of the irrigation management change is relatively limited within the entire study area. Also, by comparing the areas characterized by higher recharge differences with the calibrated spatial distribution of hydraulic conductivity, it seems that a combination of high K_s and irrigation transition is required to result in a significant impact, while irrigation transition alone is not sufficient.

The results presented here should be regarded as preliminary and require further corroboration, which will be the main objective of the next research activities.

4.3

This activity summarizes four contributions, previously indicated as

- A 3.3.7 Morphological and physico-chemical characterization of selected soil profiles in a test site to evaluate the secondary salinization processes, induced by irrigation with saline waters pumped from groundwater, of soils in coastal areas.
- A 3.3.8 Hydraulic characterization of selected soil profiles in a test site to evaluate the secondary salinization processes, induced by irrigation with saline waters pumped from groundwater, of soils in coastal areas..
- A 3.3.9 Physically based dynamic simulations with a 1D agro-hydrological model, using as inputs the soil properties acquired in A.3.3.10 and in A.3.3.11, which returns a series of spatio-temporal outputs essential for quantifying the distribution of water and salts along the soil profile and the related percolation flows towards the aquifer. The simulations will be conducted considering different climatic scenarios and a progressive salinization of groundwater induced by marine intrusion.

4.3.1 Morphological and physico-chemical characterization of selected soil profiles

The selected study area is the Muravera coastal plain, located in south-eastern Sardinia (Figure 10). In this area, 36 soil profiles (Figure 10), extrapolated from the Data Base dei Suoli della Sardegna (DBSS, http://dbss.sardegnaportalesuolo.it/, authorization required) were selected to evaluate the secondary salinization processes. Moreover, data from 187 sampling sites (0-40 cm depth) were also extrapolated from DBSS.

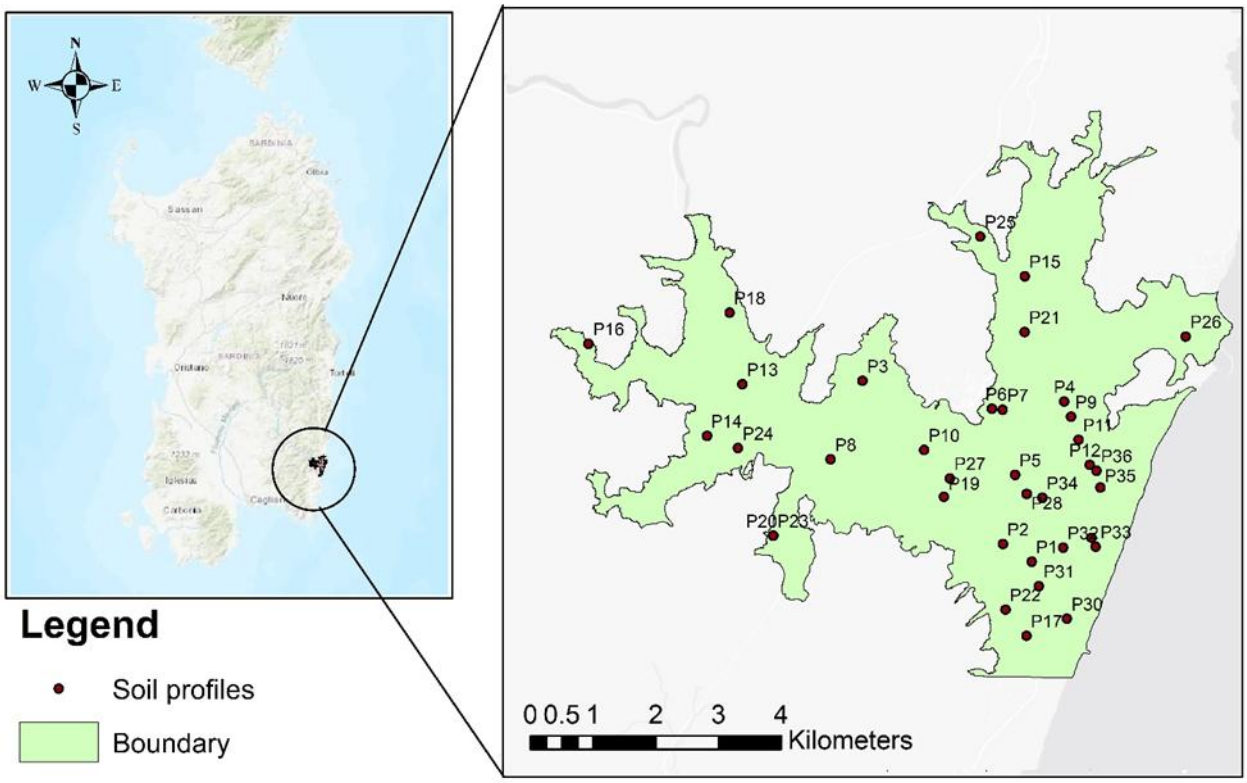

Figure 10. Study area (in green) and the investigated soil profiles.

All the morphological and physico-chemical data were organized in Excel files. Figure 11 shows the distribution of prevailing soils in the study area, while Table 1 reports the grouping of soil profiles for each map unit. Soil names in Figure 11 and Table 1 are according to IUSS Working Group WRB (2022). Most soils are derived from Holocene alluvial deposits and are characterized by a A-Bw-C horizon sequence and classified as Cambisols. These are deep soils, mostly with a texture class of loam, sandy loam, clay loam or sandy clay loam. Most of them show stratification due to the arrival of fresh material and have high base saturation (Eutric Fluvic Cambisols). In the areas closest to the coast, these soils are affected by salinity and sodicity (Eutric Fluvic Cambisols (Salic, Sodic)) (map unit B). In these areas, soils with a surface horizon, or a subsurface horizon at a shallow depth, that contains high amounts of readily soluble salts, i.e., salts more soluble than gypsum, and sodicity may also occur (Sodic Solonchaks). In the highest Holocene alluvial terraces, Cambisols with low base saturation (Dystric Cambisols) can be found, while in the plain, whenever the arrival of fresh material is affecting the mineral soil surface, Eutric Fluvisols are found. Soils derived from Pleistocene alluvial deposits are characterized by a A-Bt-C horizon sequence and classified as Luvisols. These are deep soils, mostly with a texture class of sandy clay loam to clay loam. Soils derived from sand dunes and beaches are characterized by a A-C horizon sequence and a loamy sand or sand texture class and are classified as Eutric Arenosols.

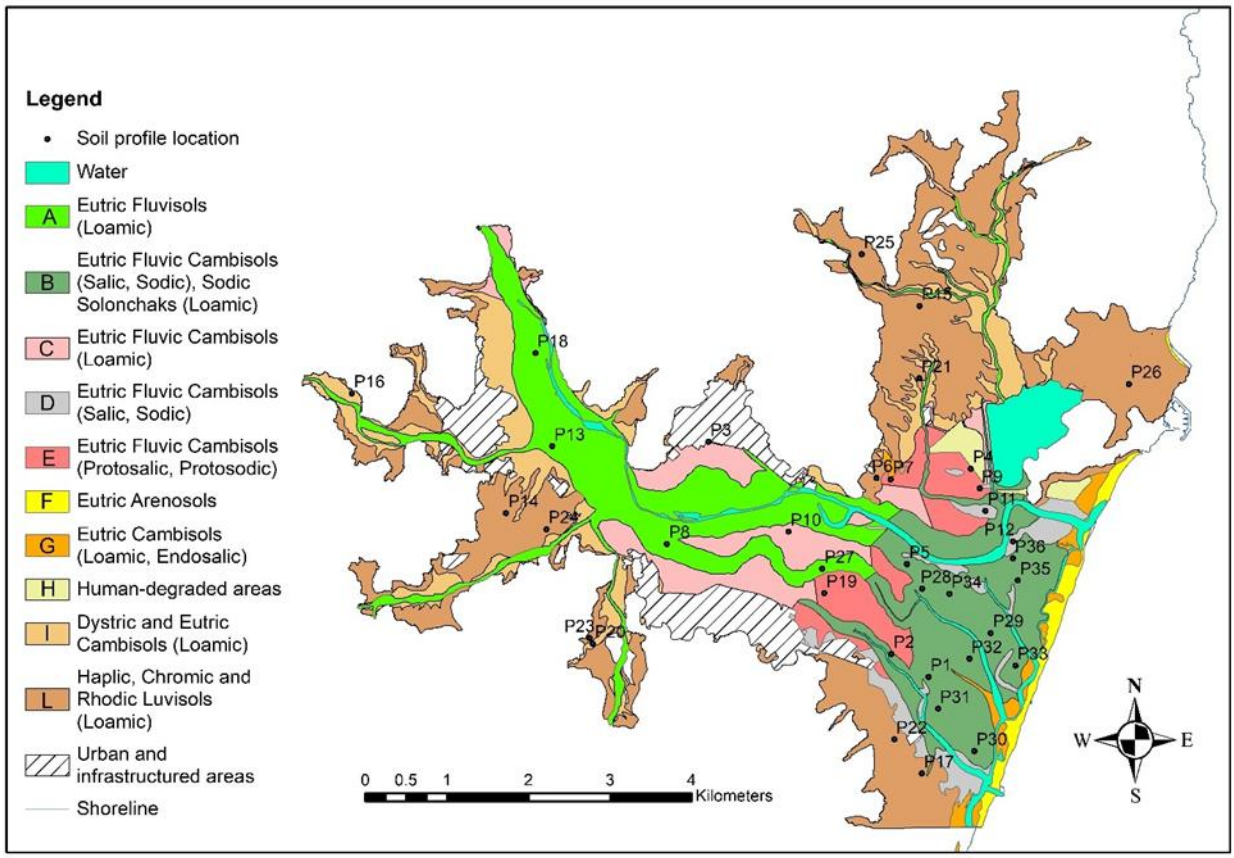

Figure 11. Distribution of prevailing soils in the study area (modified by AGRIS et al., 2014).

Table 1. Grouping of soil profiles for each map unit.

Label for soil profile groups	Soil profiles	Soil Units
A	P8, P13, P18, P27	Eutric Fluvisols (Loamic)
B	P1, P2, P5, P28, P29, P30, P31, P32, P33, P34, P35, P36	Eutric Fluvic Cambisols (Salic, Sodic) Sodic Solonchaks (Loamic)
C	P3, P10	Eutric Fluvic Cambisols (Loamic)
D	P11, P12	Eutric Fluvic Cambisols (Salic, Sodic)
E	P4, P7, P9, P19	Eutric Fluvic Cambisols (Protosalic, Protosodic)
I	P16, P20	Dystric and Eutric Cambisols (Loamic)
L	P6, P14, P15, P17, P21, P22, P23, P24, P25, P26	Haplic, Chromic and Rhodic Luvisols (Loamic)

4.3.2 Hydraulic characterization of selected soil profiles

The soil data for the study area (the Muravera coastal plain, in south-western Sardinia) were taken from the Data Base of Sardinia's soils (AGRIS Sardinia Agency, Portale del suolo, http://dbss.sardegnaportalesuolo.it/, authorization required). It is a comprehensive dataset including soil information from 223 sites, with 187 specifically focusing on the surface layer (the Ap horizon), from 0 to 40 cm depth, and the remaining focusing on 36 soil profiles, each spanning two to six different horizons, with variables depths, from 60 to over 365 cm. The soil data file encompasses a variety of morphological, physical, and chemical properties, including data on thickness, soil texture, available water capacity, and more.

In this investigation, raster layers for sand, silt, and clay were created using data from all 223 soil sites within the 40 cm surface layer. The ordinary Kriging interpolation method in GIS was applied to produce each raster layer, as depicted in Figure 12. This methodology provides a detailed representation of soil texture in the soil surface horizon across the study area.

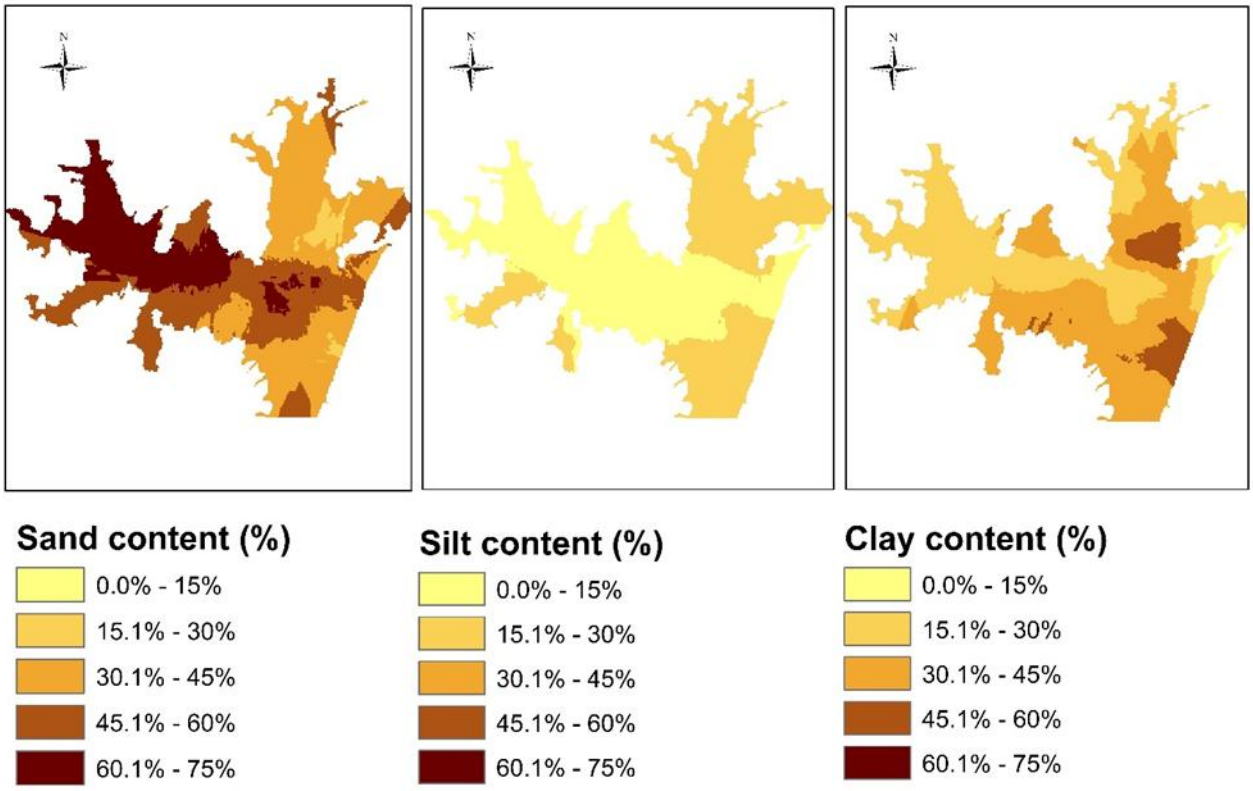

Figure 12. Sand, silt, and clay content of the surface horizon produced by ordinary Kriging.

The pedotransfer function (PTF), known as ROSETTA (Schaap et al., 2001), was used for estimateng soil hydraulic properties, leveraging the online resource provided at https://www.handbook60.org/rosetta/result. Within this study, the estimation of soil hydraulic properties was predicted on key factors such as soil texture, along with bulk density, wilting point, and field capacity. This method expeditiously provides information for saturated water content, residual water content and the other shape parameters of the van Genuchten-Mualem (Mualem, 1976; van Genuchten, 1980) unimodal soil water retention function and hydraulic conductivity.

To simulate solute transport, dispersivity, λ, values have also to be available for every soil horizon of each soil profile. As there were only limited measurements in the dataset for the area under study, we opted for deriving dispersivity values by applying the method proposed by Scotter and Ross (1994), which deduces breakthrough curves of a tracer at a given depth for a given soil starting by its hydraulic conductivity curve (Bancheri et al., 2021; Coppola et al., 2014).

In the present time, a validation of the estimated hydraulic properties is being carried out by using a fast in situ infiltrometer measurement method based on the use of Time Domain Reflectometry (TDR) (Sohbani et al.,

2023) and inversion of a 3D Richards equation to describe the time evolution of water content below a point water source.

4.3.3 Physically-based dynamic simulations with a 1D agro-hydrological model

Physically-based dynamic simulations with a 1D agro-hydrological model, using as inputs the soil properties acquired in A.3.3.7 and in A.3.3.8, which returns a series of spatio-temporal outputs essential for quantifying the distribution of water and salts along the soil profile and the related percolation flows towards the aquifer. The simulations will be conducted considering different climatic scenarios and a progressive salinization of groundwater induced by marine intrusion.

The model FLOWS (FLOw of Water and Solutes in heterogeneous agro-environmental systems) used in this study is a 1D dynamics physically-based agro-hydrological numerical model, which allows to simulate the fluxes of water and solute in the soil-vegetation-atmosphere system by accounting for all the possible interactions among soil properties, vegetation parameters, groundwater depth, and climate conditions (Coppola et al., 2009, 2012, 2014, 2015, 2019). The model simulates water flow and solute transport in the unsaturated zone respectively solving the Richard equation (RE) and the Advection-Dispersion equation (ADE). In this specific study, the model was applied to predict transport of a conservative solute input at the soil surface through the soil profile to the groundwater. Specifically, travel times needed for 25%, 50%, 75%, and 100% of the applied solute mass were calculated by using as input a wide dataset including soil horizons and related soil hydraulic properties of 36 soil profiles, average annual soil profile depth to the groundwater table (ranging from 1 to 44,58 m), climatic time series data of rainfall and evapotranspiration in the Muravera coastal plain (south-east Sardinia).

The soils in the area all formed on different alluvial sediments. The soil profiles examined are characterized by diverse textural layers varying significantly in number, sequence, and thickness across profiles. The FLOWS model allowed addressing this complex vertical variability, by simulating water flow and solute transport individually for each profile, taking into consideration the local arrangement of textural layers. Table 1 reports the travel times to the groundwater (GW) for each of the soil profiles investigated.

Table 2. The table reports the travel time (in years) required for the 25, 50, 75 and 100% of the specific input mass (M0=0.01 g/cm^2) to reach the GW, for the profiles where the depth to GW is lower than 10 m.

Soil Unit	Profile	Depth to GW (m)	TT: 25% of total mass	TT: 50% of total mass	TT: 75% of total mass	TT: 100% of total mass
A	P13	7.05	5.72	6.32	6.42	10.92
A	P18	3.70	2.30	2.45	2.72	3.04
A	P27	4.46	1.77	1.96	2.04	2.33
A	P8	2.26	1.88	2.07	2.15	2.90
B	P1	1.85	2.03	2.11	2.25	3.09
B	P2	1.25	0.87	0.89	0.91	1.75
B	P28	2.96	2.90	2.92	2.95	3.44
B	P29	1.00	0.92	0.98	1.02	2.10
B	P30	1.00	0.69	0.77	0.84	0.98
B	P31	2.00	1.81	2.02	2.08	2.89
B	P32	1.00	0.84	0.87	0.88	1.40

B	P33	1.00	0.83	0.85	0.87	1.12
B	P34	2.00	1.13	1.42	1.91	2.86
B	P35	2.00	1.12	1.28	1.61	2.86
B	P36	2.00	1.81	2.01	2.08	2.89
B	P5	2.47	2.33	2.84	2.89	3.21
C	P10	2.47	1.98	2.08	2.16	2.90
C	P3	2.14	2.30	2.88	2.88	3.19
D	P11	2.00	2.08	2.18	2.41	3.03
D	P12	3.16	2.51	2.90	2.91	3.21
E	P19	10.20	4.52	4.79	4.93	6.03
E	P4	1.53	1.22	1.75	2.00	2.88
E	P7	4.69	4.10	4.26	4.47	5.49
E	P9	1.50	1.01	1.08	1.19	2.85
I	P16	36.00	18.22	18.49	18.77	20.41
I	P20	44.58	35.34	35.89	36.44	39.04
L	P14	23.60	15.34	15.89	16.16	18.36
L	P15	25.47	19.32	19.73	20.14	22.19
L	P17	8.00	12.75	13.89	14.12	24.05
L	P21	13.47	4.11	4.25	4.52	5.21
L	P22	8.00	14.28	17.27	21.60	40.40
L	P23	40.57	39.45	40.14	40.82	43.84
L	P24	17.09	6.85	6.99	7.26	8.22
L	P25	50.00	28.49	28.90	29.32	31.37
L	P26	5.00	2.58	2.96	3.33	4.83
L	P6	4.74	2.27	2.35	2.47	3.02

The relatively lower or higher travel times were found to be mainly related to the depth to groundwater (R^2= 0.88, 0.86, 0.83 and 0.66 for TT: 25% of total mass, TT: 50% of total mass, TT: 75% of total mass and TT: 100% of total mass, respectively). However, this relationship weakens with increasing groundwater depth and solute mass to be recovered, indicating an increasing role of the soil variability (the depths and sequence of the layers in the profile, as well as their hydrological parameters) for larger travel times, inducing quite different transport behavior (and thus travel times and shape of the breakthrough curves) even in the same soil unit. This is evident in Figure 13, showing the whole set of cumulative breakthrough curves simulated by FLOWS at 1 m depth for all the soil profiles. In the graph, the thick red curve represents the average breakthrough curve. Results showed large differences in the magnitude of the different travel times among different profiles. This is because alluvial soils exhibit highly intricate textural layering, with significant variation in thickness between horizons. Unlike other soils, the impact of textural layering on water flow and solute transport in alluvial soils may be quite critical due to sometimes abrupt transitions between different textural layers within the soil profile. By looking at the figure, a large travel time variability may be already observed at 1 m depth, with 100% mass recovery travel times ranging from 200 to 500 days. However, these differences are not simply related to the fact that the soil profiles belong to different soil units. Indeed, quite different curves were obtained for the same soil unit, suggesting that even a macroscopic uniformity of soil profiles from a pedological point of view may result in significant changes in their hydrological behavior, with quite different hydraulic properties and dispersivities of the different soil layers. For the same reasons, it is

even possible that soil profiles belonging to different soil units are characterized by similar breakthrough curves.

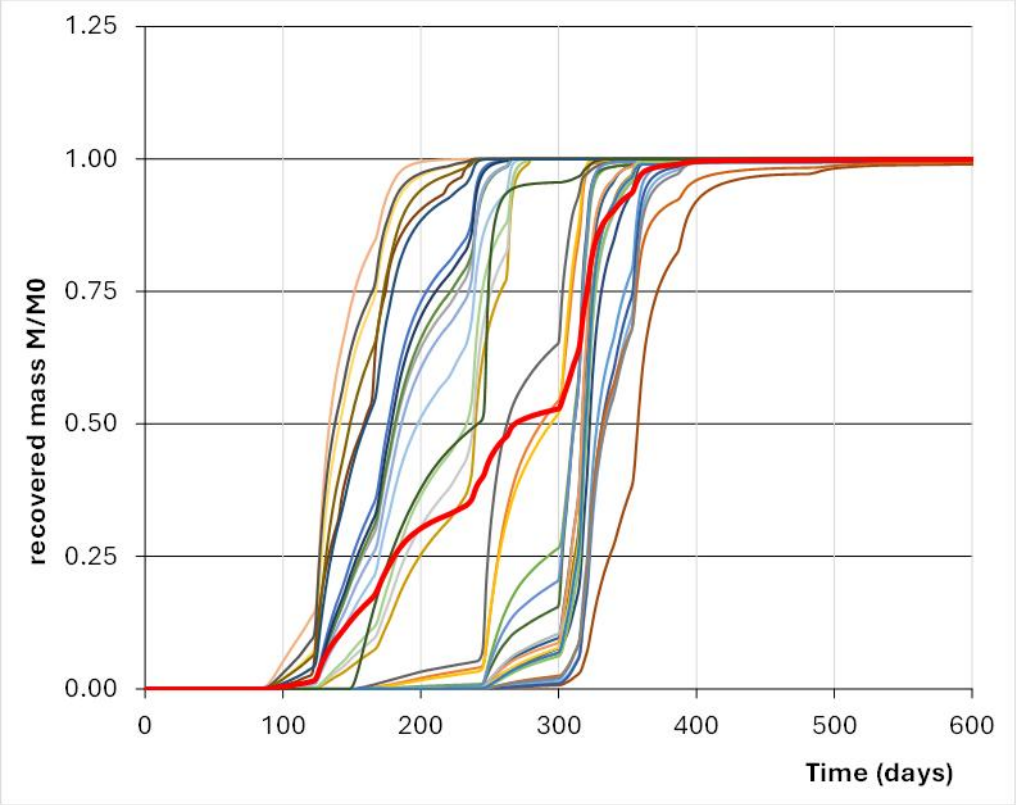

Figure 13. Whole set of cumulative breakthough curves at 1 m depth simulated by FLOWS for all the soil profiles investigated. The thick red curve represents the average curve.

5. Surface water models

This part of the activity is devoted to modelling different aspects of the hydrological cycle complexity with the inclusion of anthropogenic factors to address surface water in drought conditions. The goal is achieved through the development and calibration of surface water models for drought modelling.

5.1 Hydrological models for the quantification of hydrological drought hazards at seasonal and climatological scale in the Po watershed and Arno watershed

5.1.1 Context

Droughts transition from precipitation deficits to streamflow deficits, impacting hydrological systems and causing severe consequences for the environment, societies, and economies. As a result, robust water availability modeling across the hydrological cycle is needed for effective water management. However, classical hydrological modeling approaches typically simulate continuous streamflow time series encompassing both drought and flood events, and some studies have shown limitations in simulating streamflow droughts and their processes. Efforts to enhance the transferability of distributed hydrological models to droughts involve evaluating streamflow, actual evapotranspiration (ET), and terrestrial water storage anomalies (TWSA) during different drought conditions.

In this context, we outline here efforts to set up the spatially distributed sub-km Continuum hydrological model for the Po river basin, with a specific focus on droughts.

5.1.2 The Continuum model

The hydrological model Continuum is an open-source continuous and grid-based hydrological model (https://github.com/c-hydro). It simulates the main hydrological processes in a process-oriented but parsimonious way, by solving the mass and energy balances with up to 8 calibration parameters. The model also includes optional modules to simulate flow regulation by natural and man-made reservoirs, and other hydraulic infrastructures (water withdrawals and releases), with additional parameters to this end.

Here we set up the model to simulate snow accumulation and melting, vegetation interception, energy fluxes and evapotranspiration (ET), subsurface water dynamics, major reservoirs, and surface flow routing. The snow accumulation and melting module relies on mass conservation and a hybrid approach for snowmelt, which couples a radiative term with a temperature-driven one. Vegetation interception is simulated through an empirical equation. The dynamics of water in the soil is modelled through an adaptation of the Horton equation and in the groundwater by a modification of the Darcy law. The surface flow routing scheme is based on a Manning-type equation.

5.1.3 Model setup and calibration

We ran Continuum on a regular grid at 0.009° resolution (for a total of 212901 grid cells) and 1 hour time step. Forcing data (air temperature, relative humidity, precipitation, wind speed, and radiation) are taken from interpolation of in situ weather stations, including precipitation maps from the radar-gauge Modified Conditional Merging (MCM) algorithm (https://doi.org/10.3390/atmos12060771). We further used information from DPC and a global product for dams to derive the parameters required for the representation of reservoirs in the model (https://esajournals.onlinelibrary.wiley.com/doi/full/10.1890/100125).

Model calibration was performed using quality-checked daily mean streamflow time series for 38 sub-catchments in the Po river basin. Evaluation was further performed using evapotranspiration from the METv2 product by the Land Surface Analysis of the EUMETSAT Satellite Application Facility (LSASAF) and terrestrial water storage from the Gravity Recovery And Climate Experiment (GRACE) and GRACE Follow-On (GRACE-FO) missions. The calibration was performed first using the years 2018-2019, characterized by average precipitation conditions, and then over 2016-2017, when a moderate drought occurred in the basin. The evaluation period ranged from 2009 to 2022, where the latter year was characterized by a severe drought.

We deployed a multi-site calibration procedure to calibrate the model against discharge (Q) data (18 sub-catchments, dots with black edges in Figure 14). For calibration, we used 2-year periods, with the first 6 months for model warm-up and the remaining 1.5 years for calculating model performances. We calibrated four model parameters: the Curve Number (CN), the field capacity (ct), the infiltration velocity at saturation (cf), and a parameter regulating the baseflow from the groundwater storage (ws). CN, ct, and cf are spatially distributed parameters, while ws is lumped for the whole model domain. We set the first guess parameters from (i) global maps of soil characteristics and land cover for CN, ct, and cf , and (ii) expert knowledge for ws. We then used an iterative parallel search algorithm to optimize scaling factors for these first guess parameters. We based the cost function on a sum of Kling-Gupta Efficiency (KGE) on the daily Q of each calibration sub-catchment, weighted with the logarithm of the sub-catchment area, to emphasize downstream sub-catchments.

5.1.4 Results

Model performances for Q were comparable during wet years, moderate drought periods (Figure 15), and the whole study period for the model calibrated during average climatic conditions. Across all the sub-catchments, mean KGE (± 1 standard deviation) was equal to 0.59(±0.32) during wet years, 0.55(±0.25) for moderate droughts, and 0.7(±0.19) over the whole study period. At the basin outlet Pontelagoscuro, the model represented properly the slight decline in Q since autumn 2019 and the low Q values during the severe 2022 drought (KGE = 0.82). Nonetheless, model performances across the study sub-catchments showed a decrease during the severe 2022 drought (KGE = 0.18±0.69, Figure 15). Even though the model preserved some skill over the climatological mean, performances were low especially in the evaluation catchments and in terms of bias.

Including a moderate drought (the 2017 event) in the calibration period did not improve model skills during the severe drought (2022). Model performance during calibration was similar during both calibration experiments, with a mean KGE across the calibrated sub-catchments of 0.58 for calibration 1 and 0.44 for calibration 2 (Table S4). Also, for the model calibrated during a drought, Q simulation performances across the study sub-catchments deteriorated significantly during the severe 2022 drought compared to model skills during moderate droughts (KGE = 0.5±0.27 during moderate droughts vs 0.18±0.63 during the severe drought, Figure 16c). Furthermore, the model calibrated during a moderate drought showed issues in simulating monthly ET standardized anomalies in the croplands during the severe drought, with mean correlation coefficient r = -0.11 and mean nRMSE = 1.78 across the cropland model cells (Figure 16f and 16i), similarly to the model calibrated during average climatic conditions.

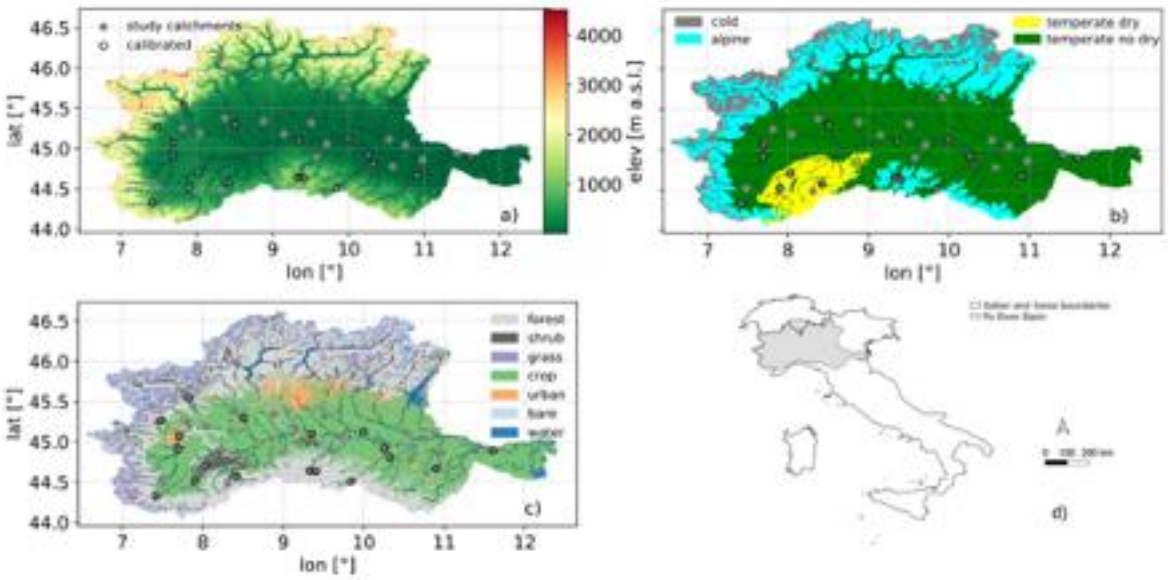

Figure 14: Overview of the study area: maps with (a) elevation, (b) climate, (c) land cover types, and (d) location of the model domain, modelled river network (dark blue line), and study sub-catchments outlets (grey dots, with black edge if used in model calibration).

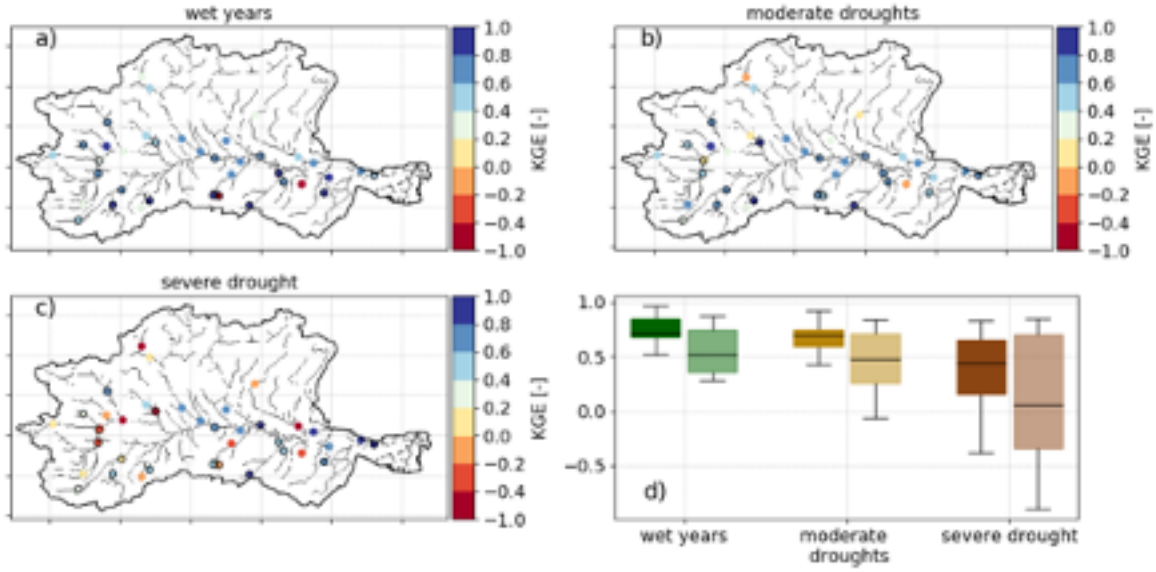

Figure 15: Streamflow (Q) model performances for the model calibrated during average climatic conditions: KGE values on monthly Q during wet years (a), moderate droughts (b), and the severe drought (c) for each study sub-catchment, and their distributions as boxplots (d) grouped by calibration (full colours) and evaluation (light colours) sub-catchments.

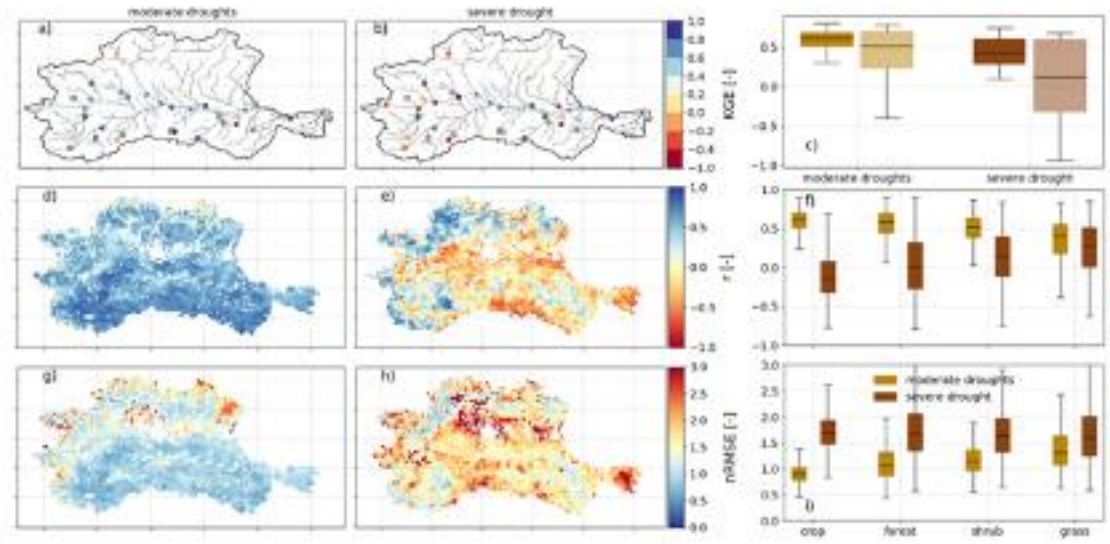

Figure 16: Summary of model performances for the model calibrated during a drought: KGE values on monthly Q over moderate droughts (a) and the severe drought (b) for each study sub-catchment, their distributions as boxplots (c) grouped by calibration (full colours) and evaluation (light colours) sub-catchments, maps of r and nRMSE on monthly ET standardized anomalies over moderate droughts (d and g) and the severe drought (e and h), and errors distributions as boxplots per each land cover types (f and i). Water bodies and urban areas were excluded from the comparison. Model outputs were rescaled by bilinear interpolation to the resolution of the LSASAF product for comparison.

5.2 River low-flow and intermittency modelling and spring modelling in North-Western Italy

In these months the research activity considered the discharge data of seven springs monitored by DIATI of Politecnico di Torino. The aim is to build a model able to predict spring discharge for different precipitation scenarios. Since the field data about the recharge catchment of each spring are very scarce, it is not possible to build a physically based model so that we optioned for a black-box model that links spring discharges with meteorological data: precipitation and temperature.

In the first step, to better understand the recharge dynamics of the spring aquifer and include in the model appropriate variables, we analyzed the relationship between indicators indexes such as Standardized Precipitation Index - SPI, the Standardized Precipitation Evapotranspiration Index - SPEI, the Standardized SnowPack Index - SSPI and the Standardized Run-Off Index - SRI, largely used in literature to evaluate the presence of meteorological-hydrological drought conditions.

In the following, as example, the determination coefficient of the regression between SRI (monthly values) and the others monthly indexes is shown for Fuse spring.

As it can be seen in the case of Fuse spring the standardized Run-off index is reasonably linked to the precipitation of the same month in autumn period.

The subsequent step dealt with the analysis of the existing correlations between spring flow rates and local meteorological parameters, such as cumulative precipitation, average temperature and snow depth (when available). This analysis was carried out to understand if it is appropriate to define of a multi-parametric model

able to estimate spring flow rates as function of the aforementioned meteorological parameters. At this aim correlation matrices were created that compared the average monthly flow rates with the relative cumulative values at 1, 2,3, 4, 5 and 6 months of meteorological parameters.

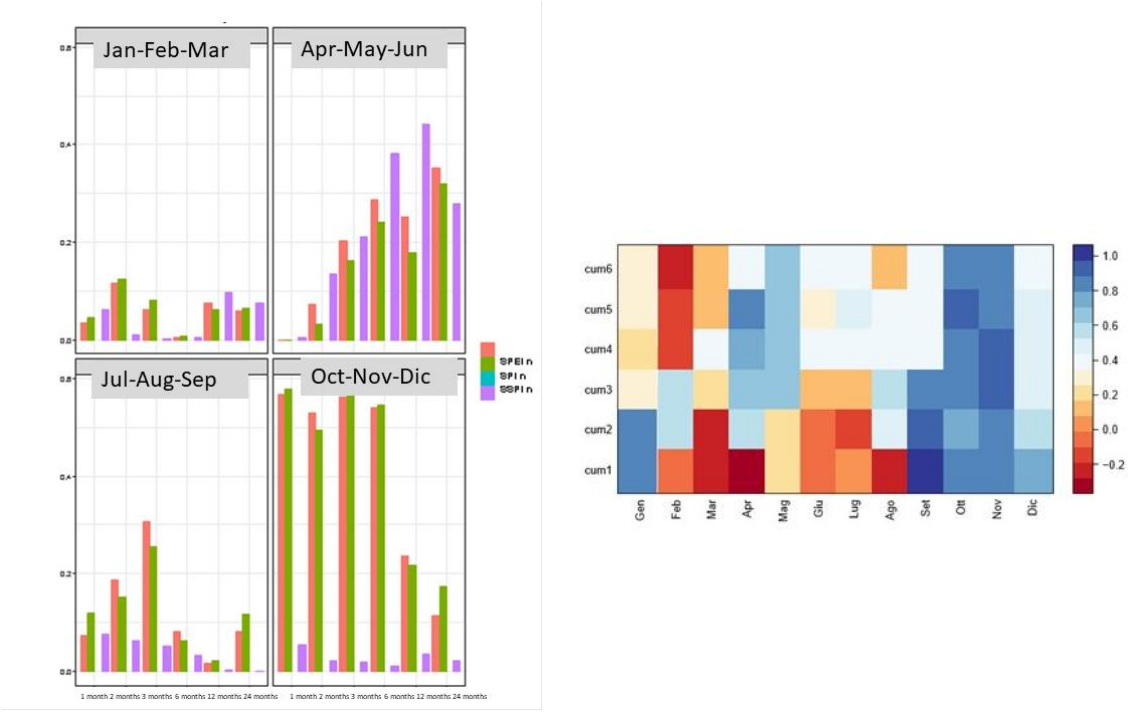

Figure 17: Left: Determination coefficient between SRI and other indexes for different seasons (Fuse case). Right: Correlation matrix between spring monthly discharge and cumulative precipitations for different period (1-6 months, Fuse case).

5.3 Development of agro-hydrological models for the quantification of agricultural drought hazards.

.5,3.1 Introduction

The definition of drought is often articulated into four types, mainly based on the variables observed and the type of impact. Meteorological drought is typically defined as a decrease in precipitation and/or increase in temperature with respect to a statistically defined normal behavior, for a given length of time. Hydrological drought is defined based on evidence of water deficit in water bodies, and usually occurs in consequence of a long-period meteorological drought. Agricultural drought is a drought that has adverse impacts on crop responses, mainly intended as crop yield reductions or crop failures. Finally, socio-economic drought refers to lack of water resource supply with respect to the water demand for given social and economic goods and services. The focus of activities A3.3.5 (Agro-hydrological models for agricultural drought hazards) and A3.4.4 (Agro-hydrological modelling for water scarcity hazard under global change scenarios) is on agricultural drought, and thus on modelling the response of cropped surfaces in Italy to water stress. The aim of A3.3.5 is to set up a modeling structure able to advance, in terms of spatial resolution, temporal resolution and extent, as well as crop identification accuracy, the knowledge of crop-specific water demands across Italy,

the meteorological water supply, and thus the deficit that would have to be compensated with irrigation where and when water is available in water bodies.

5.3.2 Model development

The starting point for A3.3.5, as a model, is WATNEEDS, a global spatially distributed process-based agro-hydrological model whose core simulates the vertical soil water balance in the active layer. WATNEEDS computes potential crop evapotranspiration based on FAO methodologies, based on climate variables and crop growth parameters. It then computes the vertical soil water balance based on the crop-specific soil cover, a set of soil parameters and precipitation data. Actual evapotranspiration is therefore computed, and green water derived, as evapotranspired water taken by the cropped surface from precipitation-generated soil moisture. Blue water, i.e., evapotranspired water delivered to the cropped surface from water bodies through irrigation, can be computed in terms of demand, as the deficit between actual and potential evapotranspiration.

With respect to the baseline version for global analyses, WATNEEDS has been made ductile in terms of processing resolution, so to accommodate higher-resolution data for analyses at country and watershed scales. Thus, WATNEEDS has been set up to work at a resolution of 30arc-seconds (ca. 650~750m resolution in Italy, depending on the latitude), incorporating higher resolution national data products instead of the baseline global ones, when they are available. The main effort in this sense has been the harmonization of different national and European crop-specific land cover datasets, which is currently being finalized. Blue water consumption for Italy for the current condition is reported in Fig.18. Further future efforts include collaborations with other activities within the RETURN project to improve the resolution and accuracy of input weather data, with respect to the ERA5 products that are currently used.

Preliminary results show the multi-level nature of the propagation from meteorological drought to agricultural drought. Changes are detected for water flows associated to this crop during past years classified as drought years and the long-term average over the period encompassing these years. In particular, even when the potential evapotranspiration increases, mainly due to increased temperatures, associated increases in effective evapotranspiration are less intense, if not absent, due to the lack in precipitation that reduces the soil moisture supply.

While these data could be directly translated into expected yield losses through yield response to water stress formulations and thus provide the basis for the next activities on drought impacts, several challenges remain as to how to attribute recorded yield losses during drought years to water stress, heat stress, and other not only biophysical, but also socio-economic factors including farmers reactions to perceived drought and drought-related normative measures.

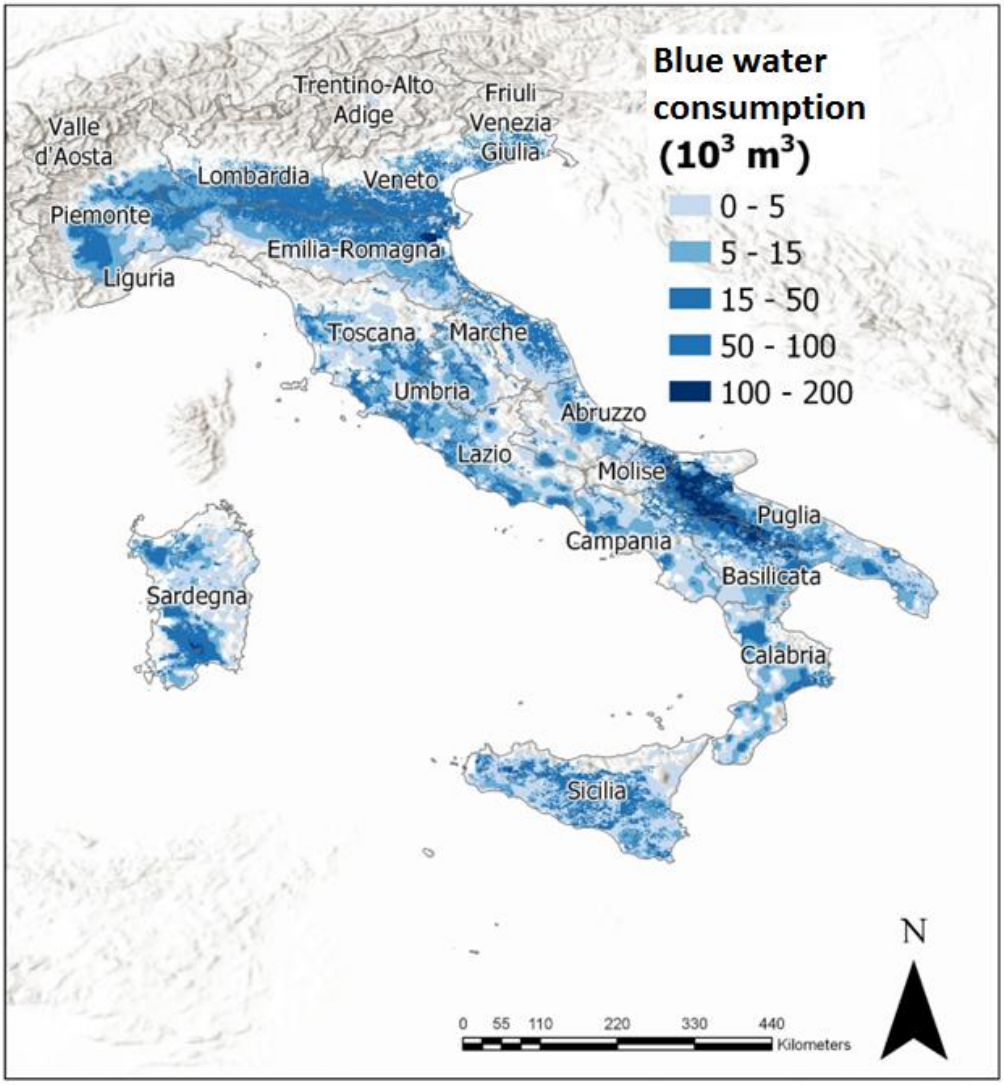

Figure 18: Blue water consumption for Italy assessed with the agro-hydrological model WATNEEDS

5.4 Modelling the hydrodynamic of the shallow regions under water scarcity conditions: during drought periods shallow regions are deeply affected by seasonal conditions

5.4.1 Introduction

The impacts of climate change on coastal lagoons are multifaceted and significant, given their position at the interface of terrestrial and marine ecosystems. These impacts are driven by a combination of increased atmospheric CO2 levels, rising temperatures, sea-level rise, and changes in precipitation and storm patterns. As a university researcher in hydraulics, I would focus on understanding how these changes affect the hydrodynamics, water quality, and ecological health of coastal lagoons. Here are the main impacts:

Changes in Salinity: Seawater intrusion into coastal lagoons can lead to higher salinity levels, particularly in regions where sea-level rise is significant. This can alter the species composition of flora and fauna within

these lagoons, harming species that are not tolerant to higher salinities. Conversely, in areas where increased precipitation dilutes lagoon waters, reduced salinity can also disrupt the ecosystem.

Altered Precipitation Patterns: Changes in the amount, timing, and intensity of precipitation can have profound effects on coastal lagoons. Increased runoff can carry more nutrients and pollutants into lagoons, leading to issues like eutrophication, which in turn can result in harmful algal blooms and dead zones. Reduced precipitation can lower water levels, which may concentrate pollutants and affect water quality negatively.

Temperature Changes: Rising temperatures can affect water temperatures in coastal lagoons, influencing the metabolism, growth rates, and distribution of aquatic organisms. Temperature impacts also extend to altering the stratification of water columns and the oxygen levels within the lagoon, both of which are crucial for sustaining healthy ecosystems.

Sea-level Rise: This is perhaps the most direct impact of climate change on coastal lagoons but it can be of moderate importance depending on the geometric characteristics of the lagoon. As sea levels rise, lagoon water levels increase in turn thus opening connections between the open sea and the lagoon that were dry in the recent past. This can lead to flooding of surrounding low-lying areas and loss of habitat for terrestrial species and for aquatic species. Additionally, the change in water levels can alter the hydrodynamics of lagoons, affecting circulation patterns, residence times of water, and salinity gradients.

Extreme Weather Events: With climate change, the intensity and frequency of storms and hurricanes are expected to increase. Such events can cause dramatic changes in coastal lagoons, including breaches of barrier systems, changes in sedimentation patterns, and significant impacts on water quality and ecosystem structure.

Considering that climatic models can provide forcing conditions at a large scale but the effect on water quality and the environmental matrixes can be evident at a much smaller scale, hydrodynamic models can effectively downscale the impact of climate change on lagoons.

5.4.2 Materials and methods

The hydrodynamics of the lagoon will be analysed using the 3D numerical model PANORMUS (PArallel Numerical Open-souRce Model for Unsteady flow Simulation), developed at the University of Palermo. The numerical model has been widely validated in environmental engineering applications (see, among others, De Marchis and Napoli, Adv Water Resour, 31:1662–1673 and Napoli et al., Bound-Lay Meteorol, 123(1):159–175). The numerical simulations will allow to analyse first the hydrodynamic circulation inside the Stagnone lagoon in the actual conditions, with water mixing guaranteed only by the water flowing through the northern and southern mouths. Field measurements will be necessary to corroborate the proposed numerical model. The collected data will further analyse the hydrodynamic circulation inside the lagoon and the flushing capability when the channels are obstructed.

The marine environment was modelled by means of the fully 3D numerical model PANORMUS (PArallel Numerical Open-souRce Model for Unsteady flow Simulation). The PANORMUS is an in-house finite-volume model and is able to solve the Reynolds-averaged momentum and mass balance differential equations on a curvilinear structured grid. The incompressible Reynolds Averaged Navier-Stokes and continuity equations, in the summation convention formulation, read:

$$\frac{\partial u_i}{\partial t} + \frac{\partial u_i u_j}{\partial x_j} - \nu \frac{\partial^2 u_i}{\partial x_j \partial x_j} + \frac{\partial p/\rho}{\partial x_i} + \frac{\partial \tau_{ij}}{\partial x_j} + g \frac{\rho}{\rho_a} \delta_{i3} + f_i = 0 \qquad i, j = 1,..3 \qquad (1)$$

$$\frac{\partial u_i}{\partial x_i} = 0 \quad i = 1,..3 \qquad (2)$$

where t is the time, x_i the *i-th* axis (with the east-west, north-south and vertical directions aligned with the axes x_1, x_2 and x_3, respectively), u_i the i-th component of the Reynolds averaged velocity, ρ the water space dependent density, ρ_a the reference density, p the Reynolds averaged pressure, g the gravity acceleration, ν the kinematic viscosity, δ_{ij} the Kronecker delta, f_i the i-th component of the Coriolis acceleration and τ_{ij} the Reynolds stresses.

As specified above, the turbulent Reynolds stresses τ_{ij} are modelled using the k – ε turbulence model in the 'standard' formulation (Launder and Spalding, 1974). Specifically, the isotropic eddy viscosity νt is obtained as $\nu_t = c_\mu k^2/\varepsilon$, where c_μ is a closure parameter and *k* is the Turbulent Kinetic Energy (TKE) and ε the dissipation rate of the TKE (for details see, De Marchis and Napoli, 2008).

In order to simulate coastal processes the free surface movements, mainly given by tidal oscillations of low frequency and relatively high amplitude and by low amplitude oscillations (with higher frequency) typical of the wind seiche motion, are calculated according to the kinematic *boundary condition*:

$$\frac{\partial h}{\partial t} + u_{1,s}\frac{\partial(h + z_B)}{\partial x_1} + u_{2,s}\frac{\partial(h + z_B)}{\partial x_2} - u_{3,s} = 0 \qquad (3)$$

where $u_{1,s}$, $u_{2,s}$ and $u_{3,s}$ are the velocities at the free surface along the x_1, x_2 and x_3 directions, respectively.

Since the water mass is bounded on the top by a free surface, the pressure can be calculated according to:

$$p = g\,\rho_a\,(h - x_3) + \rho q \qquad (4)$$

where *q* is the dynamic pressure. Introducing equation (4) into equation (1), it is obtained:

$$\frac{\partial u_i}{\partial t} + \frac{\partial u_i u_j}{\partial x_j} - \nu\frac{\partial^2 u_i}{\partial x_j \partial x_j} + \frac{\partial q}{\partial x_i} + \frac{\partial \tau_{ij}}{\partial x_j} + g\frac{\rho - \rho_a}{\rho_a} + \rho_a\frac{\partial \eta}{\partial x_i} + f_i = 0 \qquad i, j = 1,..3 \qquad (5)$$

In equations (2), (3) and (5), the time- and space-dependent density field is obtained through the resolution of a state equation starting from the salinity S and temperature θ fields. To obtain the S and θ fields, the conservation equations must be resolved:

$$\frac{\partial \theta}{\partial t} + \frac{\partial \theta\, u_j}{\partial x_j} - \kappa_\theta\frac{\partial^2 \theta}{\partial x_j \partial x_j} + \frac{\partial \lambda_{\theta j}}{\partial x_j} = 0 \qquad (6)$$

$$\frac{\partial S}{\partial t} + \frac{\partial S\, u_j}{\partial x_j} - \kappa_s\frac{\partial^2 S}{\partial x_j \partial x_j} + \frac{\partial \lambda_{sj}}{\partial x_j} = 0 \qquad (7)$$

where κ_θ and κ_s are the molecular diffusivity of temperature and the molecular salt diffusivity, respectively $\lambda_{\theta j}$ and λ_{sj} are the salinity and temperature fluxes. The initial values of temperature and salinity has to be chosen considering the period of simulation and the region of analysis and potential climatic scenarios.

The numerical code (Panormus) was extensively validated against laboratory results, analytical solutions and experimental observations in natural water bodies, confirming that the model is able to reproduce the hydrodynamic mixing in environmental and industrial applications (see, Napoli et al., 2008; De Marchis et al., 2010). Further details on the hydrodynamic model and on a free surface environment application can be found De Marchis et al. (2012). In order to take into account for the pollutant dispersion in the coastal regions the numerical model has to be further implemented, jointly with the system of conservation equations for momentum, to consider the mass conservation equations for any suspended or dissolved matter present in the water body, which are conveyed and diffused by the currents and by turbulence effects according to:

$$\frac{\partial C}{\partial t} + \frac{\partial\, C u_i}{\partial x_i} - \alpha\frac{\partial^2 C}{\partial x_i \partial x_i} + \frac{\partial\, \Lambda_j}{\partial x_j} - F_c = Q \qquad (8)$$

where *C* is the tracer concentration, u_i is the *i*-th component of the averaged velocity calculated according to the Reynolds averaged Navier Stokes equations (7), α the molecular diffusivity, Λ_j the turbulent diffusive flux modelled as $\Lambda_j = -\Gamma$**Errore.**, with Γ the turbulent diffusivity obtained as the ratio between the eddy viscosity ν_t and the turbulent Schmidt number. F_c is the horizontal subgrid-scale diffusion term and Q represents the source term or sink of the concentration and takes into account for the possible bio-chemical decay time with a first-order kinetic law (Crane and Moore 1986; Evison 1988):

$$Q_t = Q_0 \cdot exp(-K_b \cdot t) \qquad (9)$$

where Q_0 is the initial number of E. coli, Q_t the number of E. coli remaining at time t (days) and K_b is the die-pff rate constant. The value of Q_0 is calculated according to the catchment and sewer model and introduced as input data in the RWB model.

The computational modelling of pollution dispersion in coastal areas, using a 3D Computation Fluid Dynamics (CFD) model, is a key issue to preserve the environment of the coastal area. To take into account for a real hydrodynamic circulation in the coastal area the proper conditions have to be assigned at the boundaries. The forces driving the circulation, both variable tidal levels and wind velocity, have been considered external forces driving the current. The wind speed produces a wind shear stress over the free surface, partially responsible of the hydrodynamic circulation, which is calculated according to:

$$\tau_s = \rho_{air}\, u^{*2} \qquad (10)$$

where ρthe air is the air density, and u^{*2} is the air friction velocity at the free surface. This friction velocity can be related to the wind speed W_{10} at the standard height of 10 m and to the wind drag coefficient C_{10} through the equation:

$$C_{10} = \frac{u^{*2}}{W_{10}^2} \qquad (11)$$

The wind drag coefficient is calculated by the widely employed Wu's formula (Wu, 1982):

$$C_{10} = (0.8+0.065W_{10})\cdot 10^{-3}. \qquad (12)$$

The Italian wavemeter and meteorological network registered the wind speed and direction imposed in the RWB's hydrodynamic numerical simulation.

5.4.3 A potential case of use to start testing: Stagnone di Marsala (Sicily)

The lagoon of Stagnone, located in front of Marsala town (Sicily), is an important natural reserve from both ecological and economic points of view. The lagoon is about 11 km long (in the north-south direction) and about 2.5 km wide (in the east-west direction). It is enclosed between the Sicilian coast and the island Isola Grande. The lagoon is connected to the Mediterranean sea through the northern and southern mouths. The mouth located in the northern part of the basin is about 400 m wide with an average depth of only 0.3–0.4 m. The shallow water thus limits the volume exchanges between the northern part of the lagoon and the open sea. To increase the local flushing capability, a 15 m wide and 1.0 m deep artificial channel was dredged in the past, parallel to the west coast of the northern mouth. On the other side, the southern inlet, characterized by a wide mouth of about 2.9 km and a depth between 1.0 and 1.50 m, ensures the mass exchange between the open sea and the lagoon, allowing for water mixing. The mean water depth in the basin is about 1.0 m, with minimum and maximum values approximately of 0.20 and 3.00m, respectively.

Two small islands, Mothia and Santa Maria, are located in the central and northern parts of the lagoon. A very small island, called Scola, is also present in the central region of the lagoon, besides an ancient submerged road connecting the Mothia island with the Sicilian coast in the south-north direction.

The lagoon's hydrodynamic circulation is predominantly driven by tidal and wind forces; episodic watershed runoff, mostly occurring during the rainfall season, is also negligible. Two main species of seagrass partially cover the sandy bottom. The northern part is characterized by Cymodocea nodosa, while the central-southern region is covered by Posidonia oceanica, which sometimes emerges during low tide.

The great naturalistic interest of the lagoon in the Mediterranean Sea is mainly due to the presence of typical vegetal and animal species. The lagoon ecosystem requires a strong water exchange rate to survive, but, unfortunately, during the last decades, the lagoon's connection with the open sea became insufficient due to bottom uplift and strong sedimentation near the northern mouth. The particular topography and interaction of driving forces make the lagoon hydrodynamics highly complex, thus motivating the use of accurate 3D modelling.

5.5 Quantifying the drought hazards via multivariate statistics, and analysis of specific drought events.

5.5.1 Introduction

Droughts can be considered one of the most severe and complex weather-related natural hazards. Despite the interlink between the spatial and temporal scales of droughts, these two aspects are often studied separately. In addition, studies usually focus on detecting the events, without trying to investigate similarities among them. In this work, we introduce a set of tools used to summarize the main properties of extreme droughts, with the goal of subdividing the events in groups characterized by similar properties. The proposed procedure allows for a drought classification that can be used for better understanding the mechanisms beyond these events.

5.5.2 Materials

The analysis is based on a dataset of drought events over Europe. Drought events were characterized in their spatio-temporal evolution following the approach proposed by Cammalleri and Toreti (2023) (10.1175/JHM-D-22-0115.1), based on a generalized 3D clustering using the Density-Based Spatial Clustering of Applications with Noise (Ester et al. 1996, 0.5555/3001460.3001507) algorithm. This approach was applied at global scale to the 3-month accumulated Standardized Precipitation Index (SPI-3) dataset derived from ERA-5 reanalysis (Hersbach et al 2020, 10.1002/qj.3803) for the period 1981-2020 as described in Cammalleri et al. (2023) (0.1038/s41598-023-30153-6). SPI-3 data updated at dekad scale are used.

Over Europe, 198 events were identified with a duration greater than 1 month and a total cumulative area of at least 350,000 Km^2. From the full European dataset of drought events, we extracted the more extreme events, i.e., the ones above a given quantile in terms of the maximum sum of SPI values reached during their duration. The threshold of the 85-th quantile was chosen and it resulted in the selection of 30 events.

5.5.3 Methodology

Temporal evolution

For each major drought, we computed the Normalized Area - Time Accumulation (NATA) curve (Chen et al. 2023, 0.1016/j.jhydrol.2023.129509). The normalized area A_{nor} at each dekad i is obtained by dividing the accumulated area at dekad i by the accumulated area at the end of the event.

The normalized duration D_{nor} at each dekad i is similarly obtained normalizing the corresponding progressive number of dekads by the total duration of the event in dekads.

$$Anor_i = \frac{\sum_{t=1}^{i} A_t}{\sum_{t=1}^{n} A_t} \qquad Dnor_i = \frac{\sum_{t=1}^{i} 1}{\sum_{t=1}^{n} 1}$$

where n is the total number of dekads in the whole event duration, and A_t is a weighted area at the time step t, given by the sum of SPI-3 values in each cell belonging to the event.

The NATA curves were fitted with a logistic function, forced to go through the (0,0) and (1,1) points. The points of the curves with maximum and minimum first derivative were used to separate each logistic curve into three phases, roughly corresponding to the early growing (phase 1), consolidation (phase 2), and exhaustion (phase 3) stages.

Spatial characterization of the events

To provide information on the spatial evolution, we combined the previous analysis with the following one on the main direction of expansion of the events. For each drought, we computed the centroid of the drought area at any given time step. We successively computed the distance of each cell in a given dekad from the centroid

at the previous dekad, and we associated each cell to one of the eight slices, each centered on a main cardinal direction (N, NE, E, SE, S, SW, W, NW, Fig. 19). By using the centroid at the previous time step, we are able to evaluate how the drought area is evolving compared to the previous status (summarized by the centroid). Finally, for each of the three stages (as defined in the previous sub-section), we computed the number of cells falling in each slice considering all dekads belonging to that phase.

Figure 19: Example of the procedure adopted to summarize the main directions of evolution of an event. The two maps show the area interested by the drought in two successive time steps (namely 1 and 2), whereas the centroid at step 1 is reported over the area in step 2 to identify the expansion in each of the 8 main directions

Classification of the drought events

The temporal and spatial characteristics of the drought events derived from the analyses discussed in the previous sections were used as inputs for a classification analysis aimed at grouping the extreme drought events based on their spatio-temporal behavior. In particular, we used the K-Medoid clustering (PAM) algorithm (Kaufman and P. J Rousseeuw 2009) with the Gower distance metric (Gower 1971, https://api.semanticscholar.org/CorpusID:14736197). The degree of separation of the clustered group is analyzed with the Silhouette method (Rousseeuw 1987, 0.1016/0377-0427(87)90125-7).

5.5.4 Results

Temporal evolution

The NATA curves are reported in Fig. 20, considering all events and separating between events during the cold, warm and mixed periods. We can observe how most of the events fall between two standard deviations from the mean showing similar behavior, with the exception of 3 events. The dispersion is lower for cold events and higher for warm events and mixed periods.

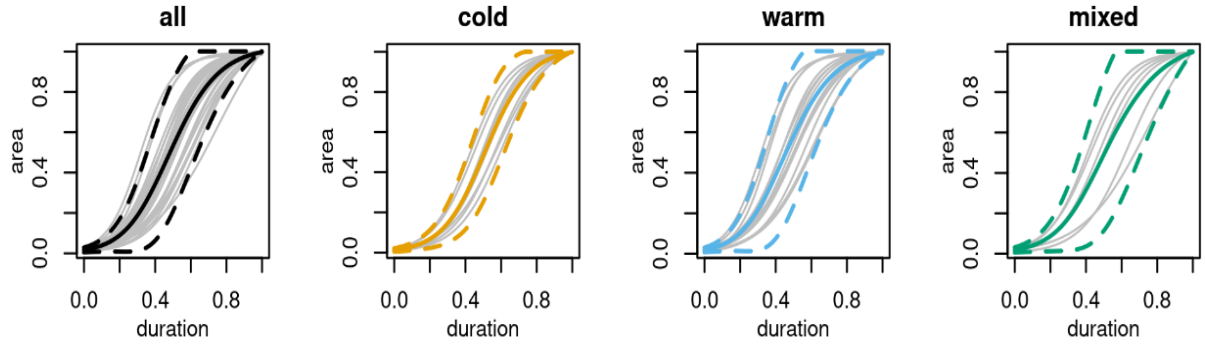

Figure 20: Normalized Area - Time Accumulation (NATA) curves for all the events, and separating between events during the cold, warm and mixed period. Grey lines represent the NATA curves for the individual events, the bold lines depict the mean behaviors, whereas the dashed lines mark +/- one standard deviation

Spatial evolution

Given the results of the analysis on the temporal evolution, the 3 events falling outside one standard deviation from the average NATA curve were removed from the spatial analysis. The reason behind this choice was to exclude events that behaved markedly different from all the others.

The investigation of the spatial evolution of droughts showed a prevalent west -- east direction, especially during the consolidation phase. The growing phase instead tends to be the one with a stronger variation in the drought extension. The exhaustion phase is usually more equally distributed across all eight directions with some exceptions.

Event classification

According to the results of the temporal and spatial analyses, we performed the PAM analysis only on the selected 27 events and using six main variables: drought duration, maximum area, average distance from the mean NATA, starting time of phase 1, starting time of phase 3 and period of the year during which the event developed (cold season, warm season, or mixed). The prevalent direction was not used in the clustering analysis due to the observed high similarity in the results for most of the events. According to the PAM cluster analysis, we subdivided the events into two groups, which were reasonably separated according to an average silhouette score of 0.3. The main characteristics of the two groups are reported in Fig 21.

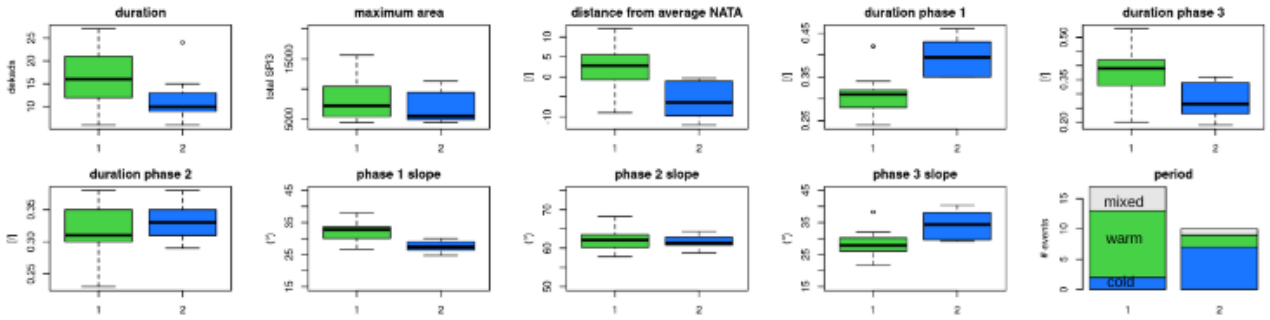

Figure 21: Characteristics of the two clusters of drought events identified using the PAM method.

The first group is comprised by warms events, characterized by longer duration, a shorter growing phase and a longer exhaustion phase. The other group of events is mostly comprised by droughts occurring during the cold season, and they tend to have shorter duration, a longer growing phase and a shorter exhausting phase. They are also less numerous (9 against 13 warm events).

Some differences can be seen also in the starting position of the events in the two groups as reported in Fig. 22. The events in group 1 start predominantly from Russia and nearby countries and from Western Europe. The events of group 2 start predominantly from eastern Europe.

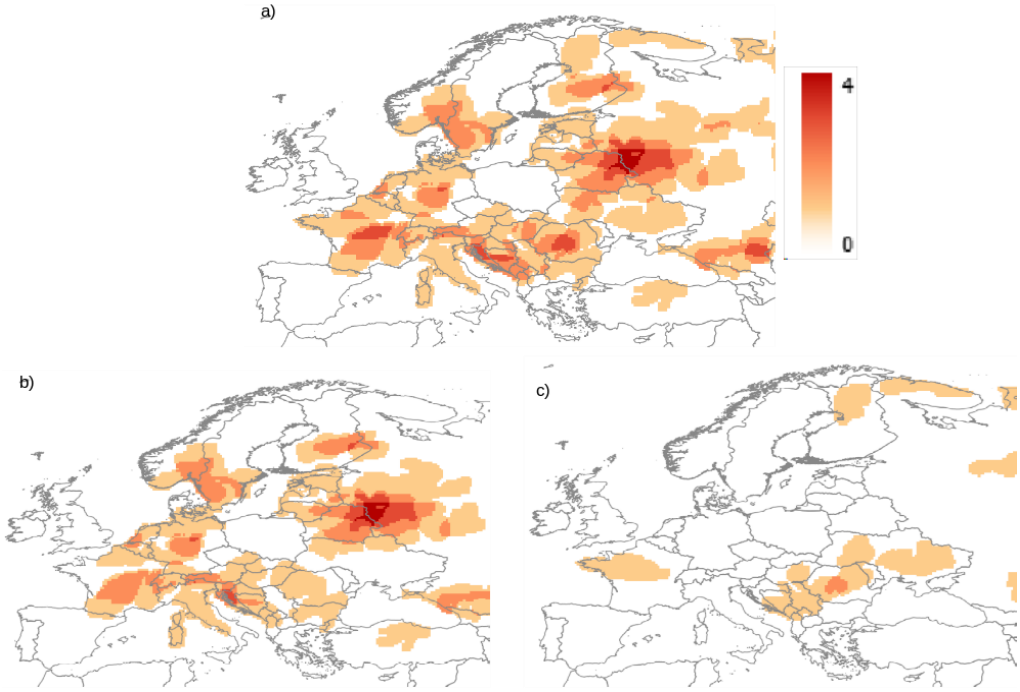

Figure 22: Starting location of drought events: a) all events, b) events of group 1, c) events of group 2

5.6 Development and integration trough machine learning of model ensembles informed by HR remote sensing products for understanding drought formation process (snow drought versus increased evaporative demand) in Alpine regions (i.e. Adige catchment).

5.6.1 Overview

Model-based drought monitoring in hydrology aims to assess and predict drought conditions through three main steps: i) hydrological modeling to spatially map relevant hydrological state variables, ii) correlation of hydro- and meteorological variables with historical drought observations/impacts to identify patterns and/or correlations, and iii) application of the developed drought hazard modelling framework to future scenarios.

The work is organized in two phases, with one reported here and the other reported in Deliverable DV3.3.2.

5.6.2 Phase 1: Modeling for Spatial Mapping of Relevant Variables in the Adige Catchment

In the modeling phase, a distributed hydrological model will be set up with reference to the Adige catchment and will be employed to generate spatial maps of drought-relevant variables. The model requires several inputs to accurately represent the complex hydrological dynamics of the catchment:

• High-resolution digital elevation model (DEM): essential for capturing the spatial variability of terrain features within the catchment. This includes mountainous areas, valleys, and plains, which significantly influence runoff generation, soil moisture distribution, and snow accumulation patterns. The DEM currently in use is FABDEM v1.0 (FABDEM V1-0 - Datasets - data.bris), a global elevation map that removes building and tree height biases from the Copernicus GLO 30 Digital Elevation Model (DEM). The data is available at 1 arc second grid spacing (approximately 30m at the equator) for the globe.

• Land Use and Cover Data, Soil properties: Detailed land cover classifications provide information on vegetation types, land use practices, and surface characteristics. This data is used for estimating evapotranspiration rates, infiltration capacities, and land surface properties, all of which affect water balance dynamics and drought vulnerability. Soil characterization in terms of texture, depth, hydraulic conductivity, and porosity (or similar proxy information) is used to estimate soil water storage capacity, water infiltration rates, and drainage properties. Both are provided to the model in the form of parametric input informed by expert knowledge of the study area.

• Meteorological Inputs: Precipitation patterns vary spatially within the catchment, with orographic effects contributing to enhanced precipitation in mountainous areas and rain shadows in valleys. Temperature gradients influence snowmelt rates, evapotranspiration, and soil moisture dynamics. The guiding criteria for the selection of meteorological datasets were their horizontal resolution, which is crucial for reconstructing available water resources in topographically complex domains, together with the abundance of observational information, which should further reduce the bias that typically affects meteorological datasets at high elevations. Two alternative sets of data are provided to the model. Firstly, ground P and T observations at several stations: P data can be spatialized through several algorithms embedded in the model and translated into mean areal precipitation time series for each hydrological response unit. Temperature data are elaborated to obtain a single linear relationship with elevation. Alternatively, gridded precipitation (P) and mean daily temperature (T) timeseries can be used to compute model inputs. Currently data from Crespi et al. (2021) are included in the model. Data covers the Trentino – South Tyrol region entirely, thus including the portion of interest of the Adige catchment closed at the Trento Ponte S. Lorenzo stream gauging station. Data covers the 1980-2022 time window with no gaps and is provided at a ~250m horizontal resolution.

Model validation

after setup, model performance will be validated in terms of drought reproduction, including drought timing and magnitude (deficit volume). This will be achieved by comparing modelled streamflow (Q) time series with streamflow observations at 22 available stations. Time series of daily streamflow observations were retrieved from the ADO hydrological database (ADO description - Projects Database Documentation (eurac.edu)). The dataset contains streamflow records for over 1400 gauging stations spread across the Alps. The stations were selected based on data availability, quality (based on the author's knowledge of the local stream gauging stations). The stations have data spanning from 1923 to the present date, however the validation will concern only the 1992-2020 time window due to how the modelling was set up.

Mapping of hydrologic state variables: after validation, the model outputs will be used to produce maps of hydrologic state variables that are relevant to drought formation, such as snow cover and snow water equivalent (SWE), evaporation (ET) and runoff. These maps will be produced at the scale of hydrological response units. The spatial patterns of SWE and ET will be compared to those presented in similar information retrieved by other sources to improve the spatial representation of said variables.

• Snow Water Equivalent (SWE) Data: SWE measurements or estimates provide critical information on snowpack accumulation and melt dynamics, especially in mountainous regions of the catchment. SWE influences spring runoff timing, streamflow generation, and water availability during the growing season, making it a key variable for drought monitoring in snow-dominated areas. Gridded Snow Water Equivalent (SWE) time series were retrieved from the IT-SNOW dataset (Avanzi et al., 2023). Data are available on the entire Italian territory, at a daily resolution and with a horizontal resolution of ~500m, and are available from September 2010 to August 2022 (included). If longer time series are needed, a proxy of SWE can be obtained through the SSPI time series available within the ADO repository (link), available at a 5km horizontal resolution over the 1979-2022 time window. As proxy for having longer time series remote sensing derived Snow Cover Anomaly (SCA) anomaly data could be considered (Matiu et al., 2021).

• Remote sensing-derived Evaporation: these data will be derived in the context of A3.1.3 (VS1 – WP3 - Task 1), leveraging MeteoSat solar radiation and Sentinel 2/3 land surface temperature data, providing daily time series of evapotranspiration at a resolution of 20m. The time series will cover the 2017-2022 time window and the entire study area.

5.7 Coupling of seasonal forecast data and machine learning techniques for reservoir operation and management in a context of water scarcity in Sicily/Southern Italy.

5.7.1 Introduction

Effective water resource management is a crucial challenge in many Mediterranean regions, where the recurrent occurrences of droughts and water scarcity over the last few years exert significant pressure on water supply systems bounded for industrial, civil, and agricultural needs. Within this context, where artificial reservoirs are the main source for multipurpose water usage, water management decisions enhancing the efficiency and efficacy of reservoir operations becomes imperative. This can be achieved by (i) making a prediction of future water availability as accurate as possible and (ii) adapting promptly and efficiently to changes in water resources.

In recent times, many methodologies based on machine learning (ML) approaches have been increasingly used to optimize the control and management of water resources. Moreover, the exacerbation of the intensity and frequency of short-duration extreme precipitation events (Forestieri et al. 2018, Treppiedi et al. 2021), coupled with prolonged droughts and heat waves (Bonaccorso et al. 2015, Caloiero et al. 2018, Arnone et al. 2020), has amplified the complexity of water resource management in Mediterranean area. In such a context, the use of seasonal forecast (SF) data is a powerful tool for guiding strategic planning across various climate-sensitive sectors (De Felice et al. 2015, Viel et al. 2016, Essenfelder et al. 2020).

The potentiality of both data-driven models and SF data has been here used to develop a tool able to predict the reservoir volume at the midterm scale (up to six months ahead in time) using as inputs monthly precipitation and monthly air temperature provided by the SF dataset as well as water volumes stored for the previous months inside the reservoir. Forecasts of water volumes will be used as a tool to support decisions. The developed Decision Support System (DSS) will be used to implement what may be called “active monitoring” of water resources, which aims to support decision makers in making “end-user” decisions concerning water allocations and, when necessary, supply restrictions and the acquisition of additional, costly water resources.

At the present time, we developed a NARX model that has been trained and tested on four different Sicilian reservoirs; the tool has been provided to the River Basin District Authority of the Sicilian Region (AdB) to be tested and to understand how to improve it in the months to come.

5.7.2 Methods

We developed a NARX, which is a type of ANN based on the linear autoregressive model commonly adopted for input-output modelling of nonlinear systems. According to this model, the value of the dependent variable $y(t)$ at time t is calculated by means of a linear regression as follows:

$$y(t) = f(y(t-1), y(t-2), \dots, y(t-m), x(t-1), x(t-2), \dots, x(t-n)) \quad (1)$$

where $y(t\text{-}i)$ and $x(t\text{-}i)$ are the previous values of the output and the previous values of an independent (exogenous) input, respectively. The indices m and n are the so-called feedback and input delays, respectively, which define the input data that are used to predict the output of the current time series. Here, the variable $y(t)$

is represented by the reservoir volume, which depends on the climate variables that are involved in the water balance of the reservoir, i.e., precipitation, temperature (that controls both the evapotranspiration and evaporation from the reservoir's surface area), and controlled releases (i.e., withdrawal from reservoir), all represented by the input variable $x(t)$.

Since the true output is available, in the first phase, an open-loop network has been used to train the NARX. In the second phase, the NARX is converted from an open- to a closed-loop network, which is used for multi-step-ahead prediction. In this phase, each estimated output (i.e., volume) is fed back within the NARX and connected to the appropriate input to estimate the next volume value.

SFs are gridded data provided by climate numerical models (Hoskins 2013), which allow one to obtain ensembles of forecasts of climate variables covering a time window up to 6-months ahead in time. Datasets are produced and released by different climate centers. Here, the last generation of the SF system, System 5 (SEAS5), released by the European Centre for Medium-Range Weather Forecasts (ECMWF) is used. The dataset has global coverage with a spatial resolution of 1°x1°.

5.7.3 Study Area and Datasets

The potentiality of both the NARX model and SF data has been exploited to develop a system able to predict the reservoirs volume at the midterm scale in four Sicilian reservoirs, i.e., Piana degli Albanesi, Poma, Rosamarina, and Scanzano, which are strategic for the water supply of the Metropolitan City of Palermo.

Precipitation, temperature, and volume data for calibrating the NARXs have been provided by the AdB and range from 1995 to 2020 (i.e., about 25 years) for the reservoirs of Piana degli Albanesi, Poma, and Scanzano and from 2002 to 2020 (i.e., about 18 years) for the Rosamarina reservoir.

5.7.4 Preliminary Results

The NARX has been used to create the prototype of a tool, valuable especially in a context where there is a chronic data shortage, often due to the lack of instruments, scarce maintenance of the existing ones and limited circulation of information among the various bodies in charge of water resources management, and where it is not easy to correctly estimate water consumption because of multiple illegal connections and due to the age of the networks that causes severe water losses (even more than 30% in some cases according to some estimates).

Figure 23 shows the control panel of the tool. As it is possible to observe, starting from the control panel, the user can choose the reservoir to work with, the release of the seasonal forecast to use for the simulations, and the exogenous variables to be used for the calibration and the run of the model. At the present time, it is possible to choose just two configurations of exogenous variables: precipitation or precipitation plus temperature. The UNIPA group is working to further develop the model by also introducing the effects of withdrawal from the reservoirs where known. As already said, the current version of the tool has been provided to the AdB to be tested and understand how to improve it in the future.

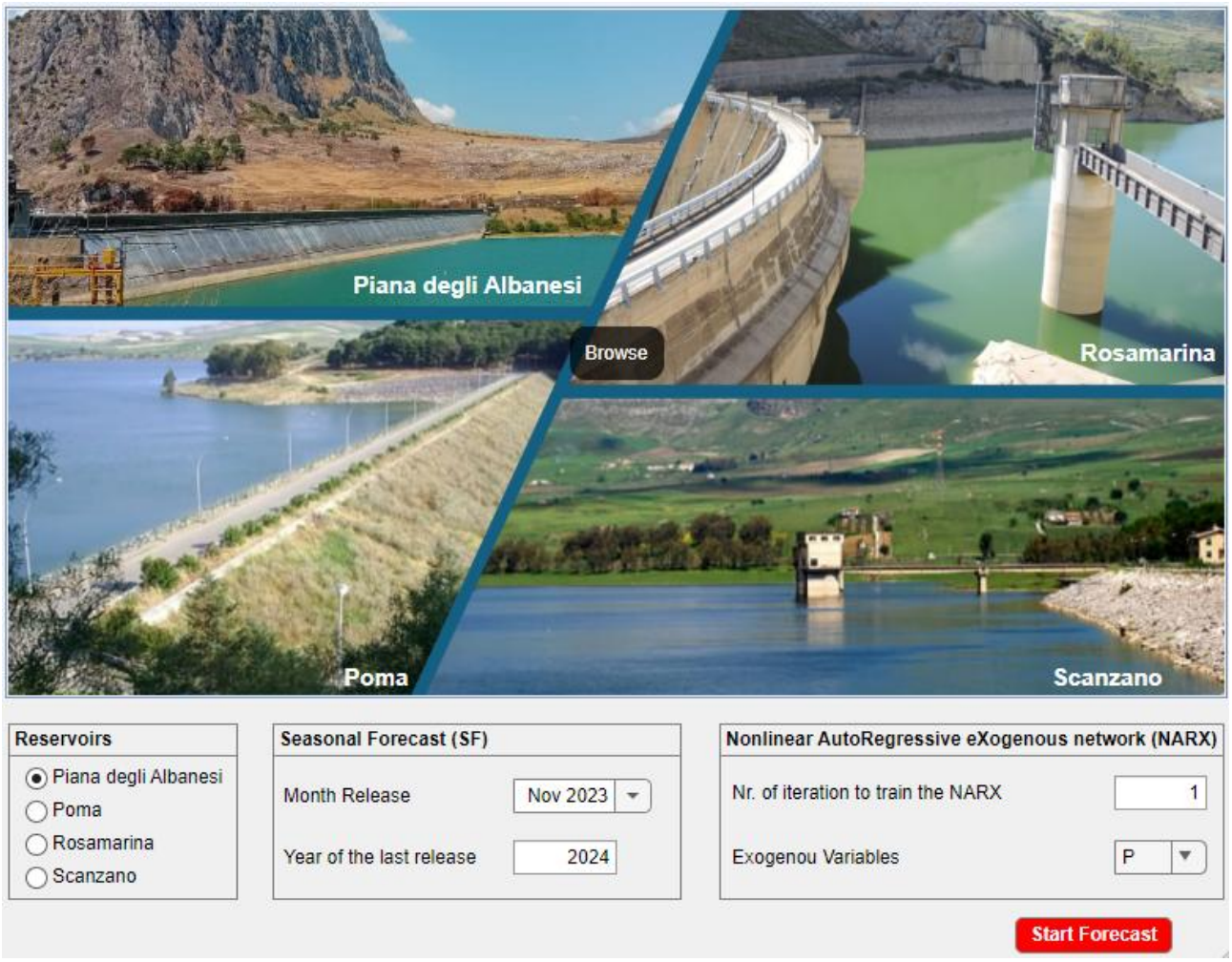

Figure 23 – Control panel of the tool developed for the AdB

Figure 24 shows some preliminary results for all the reservoirs when the NARX is forced with the SF release of September 2023. For each simulation, the initial conditions are defined by forcing the NARX with the observed monthly data up to the month at which the forecast starts. The results are provided within a probabilistic framework for the six months ahead.

As it is possible to observe, simulated volumes returned by the NARX forced with observed data (grey dashed lines) reproduce accurately the observed stored volumes (black solid lines) over the period shown. The volumes forecasted by the NARX forced with the SF data (box plots), instead, depend on the reliability of the SFs and their capability to reproduce the observed data; results are characterized by the variability inherited from the input data ensembles.

Figure 25, instead, shows the results when the NARX models are forced with the SF released in December 2023. In this case, there are not observed values for the simulated period, but, as it is possible to observe, starting from the last observed month (i.e., December 2023), the model returns, for each reservoir, always within a probabilistic framework, the water volume that is possible to have in the next six months, thus giving an indication for more aware water resource management.

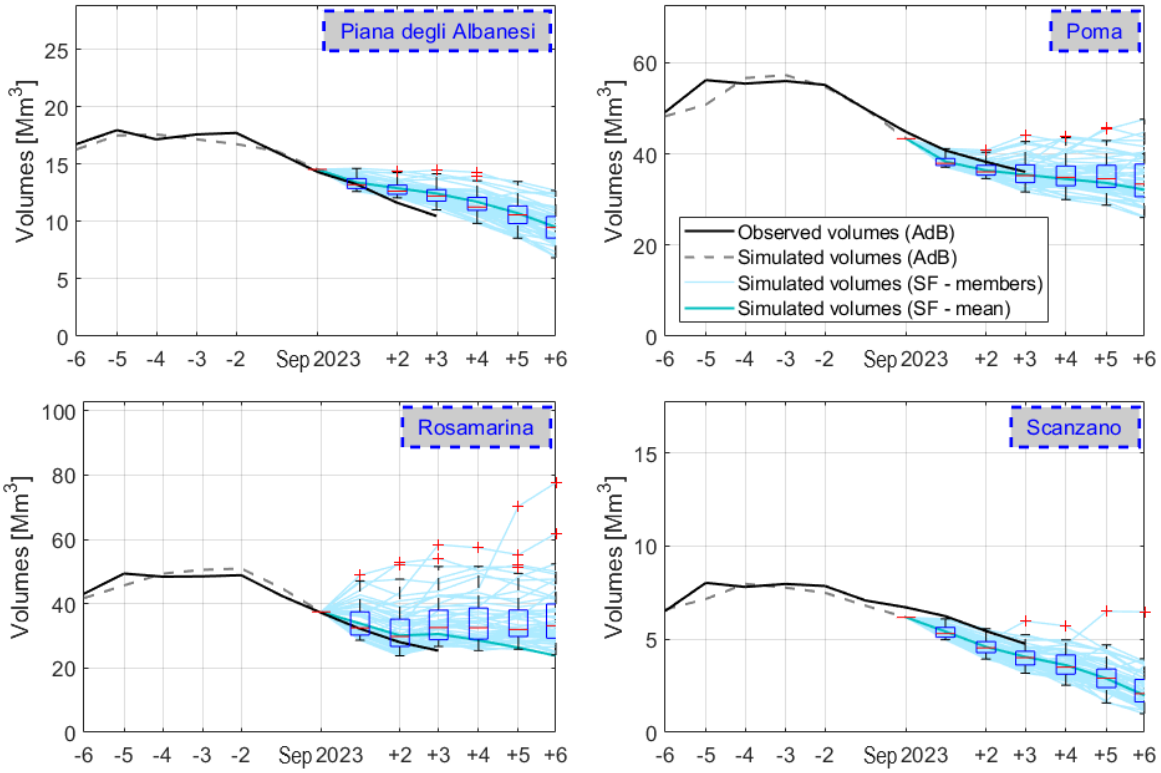

Figure 24 – NARX models results for the SF release of September 2023.

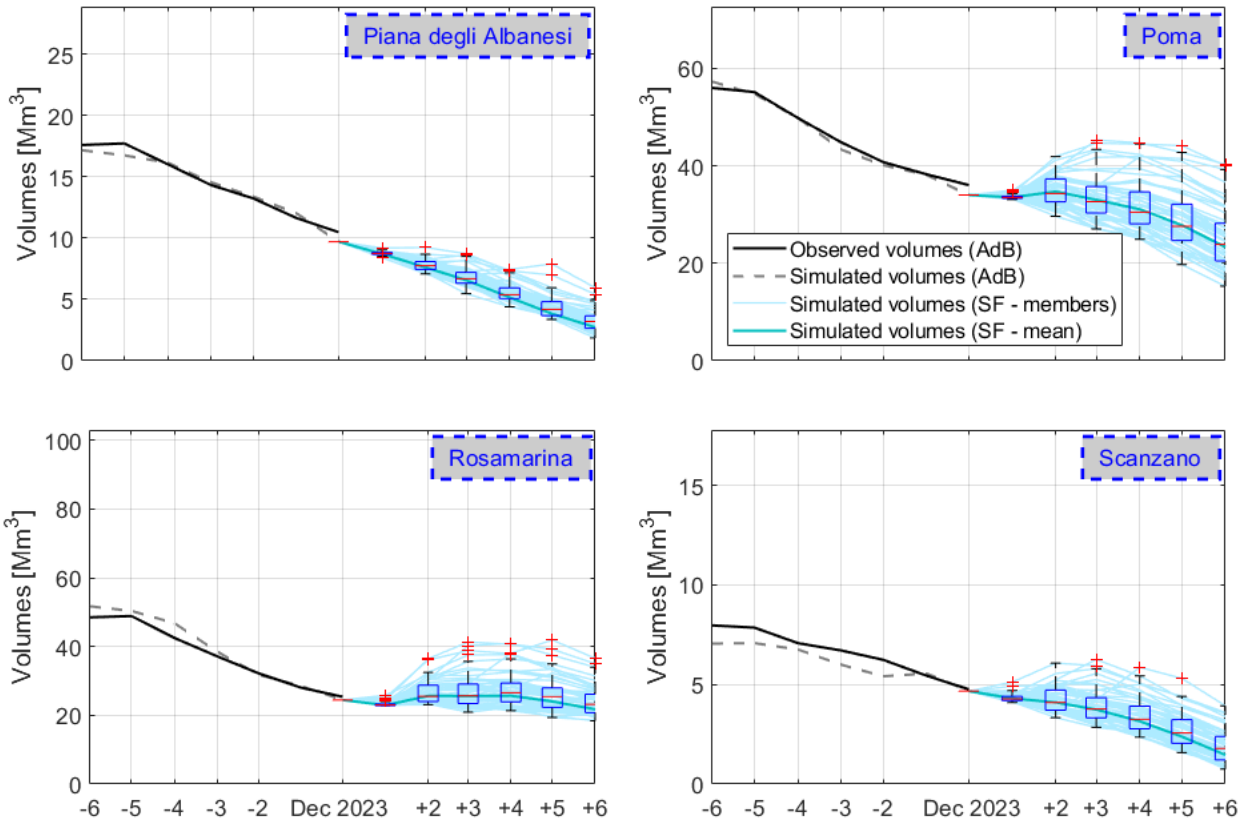

Figure 25 – NARX models results for the SF release of December 2023.

5. Conclusions

This deliverable has achieved significant advancements in understanding and managing water resources, focusing on issues such as salinization, groundwater recharge, and drought prediction.

A key area of investigation has been coastal aquifer salinization, where studies have emphasized the environmental factors contributing to saline intrusion. Through geological surveys and hydrogeological modelling in the Flumendosa plain, researchers have highlighted the impacts of withdrawals and climate change on saline intrusion, proposing methods to understand recharge sources and flow pathways. Additionally, the deliverable addressed secondary soil salinization in coastal areas, characterizing soil profiles and simulating water and salt distribution under different climatic scenarios. These studies provided critical data on water and salt dynamics and their effects on aquifer percolation.

The research also examined the impact of irrigation practices on water balance and groundwater recharge in line with the European Water Framework Directive. Utilizing the CATHY model, overland and subsurface flow was simulated in section 5.2 (activity A3.3.2), providing insights into the qualitative and quantitative effects on groundwater, which are essential for drinking water supply and irrigation. Complementing this, the use of the SWAT+ model in the Arno Basin enabled the simulation of drought conditions under various climate scenarios, focusing on agricultural variables and setting up methods for future simulations.

Agro-hydrological models were developed to quantify agricultural drought hazards across Italy, distinguishing between different drought types and focusing on those affecting crop yields. This effort aimed to create detailed models of crop-specific water demands and deficits, enhancing the accuracy and resolution of these assessments.

Tools for classifying extreme droughts were introduced, facilitating a better understanding of drought mechanisms by grouping events with similar properties. Model-based drought monitoring was another significant achievement, using hydrological modeling to map state variables, correlate hydro- and meteorological data with historical droughts, and apply these models to future scenarios for improved drought prediction and management.

Finally, the deliverable integrated seasonal forecast data with machine learning techniques to enhance reservoir management in water-scarce regions. By developing a Decision Support System using a NARX model trained on Sicilian reservoir data, the aim was to predict reservoir volumes up to six months in advance, supporting better water resource management decisions.

Overall, the deliverable showcased the synergy between various modeling techniques and data analyses, contributing to more effective water resource management and drought mitigation strategies.

6. References

AGRIS, LAORE, Università degli Studi di Cagliari, Università degli Studi di Sassari. 2014. Carta delle Unità di Terre alla scala 1:50.000 - Muravera-Villaputzu-Castiadas. http://www.sardegnaportalesuolo.it/cartografia/carte-dei-suoli/carta-delle-unita-di-terre-cut-alla-scala-150000.html (last accessed 15.05.2024).

Arnone, E., et al. (2020). Droughts prediction: A methodology based on climate seasonal forecasts. Water Resources Management, 34(14), 4313–4328. https://doi.org/10.1007/s11269-020-02623-3

Arras, C., Balia, R., Botti, P., Buttau, C., Cau, P., Da Pelo, S., Funedda, A., Ghiglieri, G., Loi, A., Lorrai, M., & Melis, M. T. (2019). Hydrogeological characterisation of the Flumendosa plain. In Flowpath 2019, National Meeting on Hydrogeology - Conference Proceedings. https://doi.org/10.14672/55260121

Bancheri, M., Coppola, A., & Basile, A. (2021). A new transfer function model for the estimation of non-point-source solute travel times. Journal of Hydrology, 589, 126157. https://doi.org/10.1016/j.jhydrol.2021.126157

Bonaccorso, B., Cancelliere, A., & Rossi, G. (2015). Probabilistic forecasting of drought class transitions in Sicily (Italy) using standardized precipitation index and North Atlantic oscillation index. Journal of Hydrology, 526, 136–150. https://doi.org/10.1016/j.jhydrol.2015.01.070

Caloiero, T., et al. (2018). Drought analysis in Europe and in the Mediterranean basin using the standardized precipitation index. Water, 10(8), 1043. https://doi.org/10.3390/w10081043

Coppola, A., Comegna, A., Dragonetti, G., & Basile, A. (2014). Mapping solute deep percolation fluxes at regional scale by integrating a process-based vadose zone model in a Monte Carlo approach. Soil Science and Plant Nutrition, 60(1), 71-91. https://doi.org/10.1080/00380768.2013.855615N

Coppola, A., Comegna, V., Basile, A., Lamaddalena, N., & Severino, G. (2009). Darcian preferential water flow and solute transport through bimodal porous systems: Experiments and modelling. Journal of Contaminant Hydrology, 104(1–4), 74–83. https://doi.org/10.1016/j.jconhyd.2008.10.004

Coppola, A., Dragonetti, G., Comegna, A., Gerke, H. H., & Basile, A. (2015). Simulated preferential water flow and solute transport in shrinking soils. Vadose Zone Journal, 14(9), 1-22. https://doi.org/10.2136/vzj2015.02.0021

Coppola, A., Dragonetti, G., Sengouga, A., Lamaddalena, N., & Comegna, A. (2019). Identifying optimal irrigation water needs at district scale by using a physically based agro-hydrological model. Water, 11(841). https://doi.org/10.3390/w11040841

Coppola, A., Gerke, H. H., Comegna, A., & Basile, A. (2012). Dual-permeability model for flow in shrinking soil with dominant horizontal deformation. Water Resources Research, 48, W08527. https://doi.org/10.1029/2011WR011376

Custodio, E. (1987). Salt-fresh water interrelationships under natural conditions. Groundwater Problems in Coastal Areas UNESCO Studies and Reports in Hydrology, 45, 14–96.

Da Pelo, S., Porru, M. C., Piscedda, F., Testa, M., Lorrai, M., Botti, P., Lobina, F., Arras, C., Buttau, C., Loi, A., Funedda, A., Biddau, R., & Cidu, R. (2022). Monitoring of physical-chemical parameter depth profile to assess sea water intrusion phenomena in a coastal multi-layer aquifer. EGU European Geosciences Union, id.EGU22-13533. https://doi.org/10.5194/egusphere-egu22-13533

Da Pelo, S., Porru, M. C., Westenbroek, S., Nielsen, M. G., & Caracciolo, D. (2021). A methodological approach for the effective infiltration assessment in a coastal groundwater. Book of Abstracts 48th IAH Congress, Brussels, Belgium, 458.

De Felice, M., Alessandri, A., & Catalano, F. (2015). Seasonal climate forecasts for medium-term electricity demand forecasting. Applied Energy, 137, 435–444. https://doi.org/10.1016/j.apenergy.2014.10.030

DSCG-STGRI. (2018). Sviluppo di una attività riguardante la realizzazione di approfondimenti idrogeologici funzionali alla valutazione dello stato quantitativo dei corpi idrici sotterranei del Distretto Idrografico della Sardegna, nell'ambito dell'aggiornamento del Piano di Gestione del Distretto Idrografico della Sardegna. Relazione Fase 2. Università di Cagliari - Responsabile Scientifico Stefania Da Pelo.

Essenfelder, A. H., et al. (2020). Smart climate hydropower tool: A machine-learning seasonal forecasting climate service to support cost-benefit analysis of reservoir management. Atmosphere, 11(12), 12. https://doi.org/10.3390/atmos11121305

Hoskins, B. (2013). The potential for skill across the range of the seamless weather-climate prediction problem: A stimulus for our science. Quarterly Journal of the Royal Meteorological Society, 139(672), 573–584. https://doi.org/10.1002/qj.1991

IUSS Working Group WRB. 2022. World Reference Base for Soil Resources. International soil classification system for naming soils and creating legends for soil maps. 4th edition. International Union of Soil Sciences (IUSS), Vienna, Austria

Mualem, Y. (1976). A new model for predicting the hydraulic conductivity of unsaturated porous media. Water Resources Research, 12(3), 513–522. https://doi.org/10.1029/WR012i003p00513

Porru, M. C. (2023). Caratterizzazione idrogeologica avanzata dell'acquifero alluvionale della piana costiera di Muravera (PhD thesis). University of Cagliari.

Porru, M. C., Arras, C., Biddau, R., Cidu, R., Lobina, F., Podda, F., Wanty, R., & Da Pelo, S. (2024). A coupled hydrogeological and multi-isotopic approach to investigate recharge, residence time and seawater intrusion in a coastal groundwater system (Sardinia, Italy). Water, 14, submitted.

Porru, M. C., Da Pelo, S., Westenbroek, S., Vacca, A., Loi, A., Melis, M. T., Pirellas, A., Bottau, C., Arras, C., Vacca, S., Mason, M. L., Lorrai, M., & Testa, M. (2021). A methodological approach for the effective infiltration assessment in a coastal groundwater. Italian Journal of Engineering Geology and Environment, 1, 183–193. https://doi.org/10.4408/IJEGE.2021-01.S-17

Schaap, M. G., Leij, F. J., & van Genuchten, M. T. (2001). ROSETTA: A computer program for estimating soil hydraulic parameters with hierarchical pedotransfer functions. Journal of Hydrology, 251, 163–176. https://doi.org/10.1016/S0022-1694(01)00466-8

Scotter, D. R., & Ross, P. J. (1994). The upper limit of solute dispersion and soil hydraulic properties. Soil Science Society of America Journal, 58(3), 659–663. https://doi.org/10.2136/sssaj1994.03615995005800030004x

Sobhani, A., Hassan, S., Dragonetti, G., Balestrini, R., Centritto, M., Coppola, A., & Comegna, A. (2023). Comparing actual transpiration fluxes as measured at leaf-scale and calculated by a physically based agro-hydrological model. Journal of Agricultural Engineering. https://doi.org/10.4081/jae.2023.1527

Van Genuchten, M. T. (1980). A closed-form equation for predicting the hydraulic conductivity of unsaturated soils. Soil Science Society of America Journal, 44(5), 892–898. https://doi.org/10.2136/sssaj1980.03615995004400050002x

Werner, A. D., Bakker, M., Post, V. E. A., Vandenbohede, A., Lu, C., Ataie-Ashtiani, B., Simmons, C. T., & Barry, D. A. (2013). Seawater intrusion processes, investigation and management: Recent advances and future challenges. Advances in Water Resources, 51, 3–26. https://doi.org/10.1016/j.advwatres.2012.03.004